

Original Article

Cite this article: Bons PD, Cao D, de Riese T, González-Esvertit E, Koehn D, Naaman I, Sachau T, Tian H, and Gomez-Rivas E (2023) A review of natural hydrofractures in rocks. *Geological Magazine* 159: 1952–1977. <https://doi.org/10.1017/S0016756822001042>










Received: 8 February 2022
Revised: 6 September 2022
Accepted: 10 September 2022
First published online: 20 December 2022

Keywords:

hydraulic fracturing; mineral veins; rock failure; Terzaghi theory; Biot theory; effective stress; fluid flow

Author for correspondence: Paul D Bons,
Email: paul.bons@uni-tuebingen.de

A review of natural hydrofractures in rocks

Paul D Bons^{1,2} , Dongsheng Cao^{2,3,4} , Tamara de Riese² ,
Eloi González-Esvertit⁵ , Daniel Koehn⁶ , Isaac Naaman² , Till Sachau² ,
He Tian^{2,3,4}  and Enrique Gomez-Rivas⁵ 

¹School of Earth Science and Resources, China University of Geosciences (Beijing), Beijing 100083, China; ²Department of Geosciences, Tübingen University, Schnarrenbergstr. 94–96, 72076 Tübingen, Germany; ³State Key Laboratory of Petroleum Resource and Prospecting, China University of Petroleum, Beijing 102249, China; ⁴College of Geoscience, China University of Petroleum, Beijing 102249, China; ⁵Departament de Mineralogia, Petrologia i Geologia Aplicada, Facultat de Ciències de la Terra, Universitat de Barcelona. C/Martí i Franquès s/n, Barcelona, 08028, Spain and ⁶GeoZentrum Nordbayern, Friedrich-Alexander University of Erlangen-Nuremberg (FAU), Schlossgarten 5, 91054 Erlangen, Germany

Abstract

Hydrofractures, or hydraulic fractures, are fractures where a significantly elevated fluid pressure played a role in their formation. Natural hydrofractures are abundant in rocks and are often preserved as magmatic dykes or sills, and mineral-filled fractures or mineral veins. However, we focus on the formation and evolution of non-igneous hydrofractures. Here we review the basic theory of the role of fluid pressure in rock failure, showing that both Terzaghi's and Biot's theories can be reconciled if the appropriate boundary conditions are considered. We next discuss the propagation of hydrofractures after initial failure, where networks of hydrofractures may form or hydrofractures may ascend through the crust as mobile hydrofractures. As fractures can form as a result of both tectonic stresses and an elevated fluid pressure, we address the question of how to ascertain whether a fracture is a hydrofracture. We argue that extensional or dilational fractures that formed below *c.* 2–3 km depth are, under normal circumstances, hydrofractures, but at shallower depth they may, but must not be hydrofractures. Since veins and breccias are often the products of hydrofractures that are left in the geological record, we discuss these and critically assess which vein structures can, and which do not necessarily, indicate hydrofracturing. Hydrofracturing can suddenly and locally change the permeability in a rock by providing new fluid pathways. This can lead to highly dynamic self-organization of crustal-scale fluid flow.

1. Introduction

Hydraulic fracturing is typically used to improve the permeability of hydrocarbon or geothermal reservoirs by further opening and propagating existing fractures and by creating new fractures to form connected networks as efficient fluid pathways (Montgomery & Smith, 2010). Reservoir stimulation by induced hydraulic fracturing started as early as the 1860s and became standard practice in industry in the late 1940s when the term 'hydraulic fracturing' came into use (Clark, 1949; Krueger, 1973; Montgomery & Smith, 2010; Gehne & Benson, 2019). The basic theory of how fluid pressure affects fracturing was developed simultaneously using the concept of effective stresses (Terzaghi, 1923, 1943; Biot, 1941; see also review of Guerriero & Mazzoli, 2021). It was then soon realized that naturally elevated fluid pressures can also induce the formation of hydraulic fractures (Anderson, 1939; Hubbert, 1951; Hubbert and Rubey, 1959; Sibson *et al.* 1975; Cox *et al.* 1986; Engelder & Lacazette, 1990). This appears particularly obvious in the case of igneous dykes, i.e. originally magma-filled fractures. With the frozen magma still preserved as the proverbial smoking gun inside the fractures, it is clear that the fluid 'magma' caused or at least played a significant role in the formation, opening and propagation of the fractures. Theory on the formation and propagation of magma-filled fractures rapidly developed from the 1970s (Weertman, 1971; Spence & Turcotte, 1985; Takada, 1990; Rubin, 1995). It is, however, of interest to note that the pioneering paper by Weertman (1971) derived its theory from water-filled crevasses in ice. It is currently widely accepted that fluid pressure must be considered for brittle deformation in fluid-bearing rocks. Although magma-induced hydrofracturing has made a significant impact on hydrofracture theory, we here focus on non-igneous hydrofracturing by aqueous fluids. A difference with magmas is that aqueous fluids are rarely sourced from a single large volume, such as magma chambers for igneous hydrofractures, and that aqueous fluids do not freeze like a magma, but may leave traces by mineral precipitates or wall rock alterations (see review by Oliver and Bons, 2001). For reviews that include igneous hydrofractures, the reader is referred to Gudmundsson (2011) and Rivalta *et al.* (2015).

© The Author(s), 2022. Published by Cambridge University Press. This is an Open Access article, distributed under the terms of the Creative Commons Attribution licence (<http://creativecommons.org/licenses/by/4.0/>), which permits unrestricted re-use, distribution and reproduction, provided the original article is properly cited.

It was only around 1960 that the term ‘hydrofracture’ as an alternative to ‘hydraulic fracture’ appeared, first in the literature of the former USSR (e.g. Soloyev & Kobeleva, 1960). Since then, the term has become popular in the literature on natural fluid-pressure induced fractures. In the literature related to oil and gas exploration and production, the term ‘hydraulic fracture’ remains mostly used. ‘Fracking’ is as an alternative term for ‘hydraulic fracturing’ that has already been in use for at least 60 years (e.g. Rogatz, 1961) but more recently gained negative connotations.

In this paper we provide a review of natural fluid-induced fractures. We first provide definitions of relevant terms in Section 2. In Section 3 we discuss the theory on hydrofracture formation and subsequent propagation. As hydrofractures are fractures formed by elevated fluid pressure (strict definition discussed below), recognizing such fractures is important to potentially infer elevated palaeofluid pressures. In Section 4 we therefore address the question of how to recognize a fossil hydrofracture in the geological record. We consider two aspects: first the geological conditions in which fractures can only form when the fluid pressure is elevated and, second, which types of fractures and mineral veins indicate hydrofracturing by their geometry, internal structures or network properties. As the formation of hydrofractures can dramatically change the local effective permeability, we finally address fluid flow associated with hydrofracturing in Section 5.

2. Definitions

In this paper we use the term ‘hydrofracture’, but the reader should bear in mind that, as far as the rock is concerned, it is the same as ‘hydraulic fracture’ as a rock ‘does not know’ whether the fluid pressure it experiences is natural or human-induced. A ‘fracture’ is a discrete planar discontinuity in a solid, such as a rock, along which cohesion or continuity across that surface is lost. The process of losing cohesion, i.e. breaking, is called ‘failure’. Please note that here we exclude so-called ductile fractures, which are interpreted to form by the collapse, linkage and coalescence of microvoids and microcracks during creep deformation, i.e. in a rock that dominantly deforms by ductile flow (e.g. Regenauer-Lieb, 1999; Gomez-Rivas & Griera, 2012). Failure ensues when the stress state in the material reaches conditions that the material cannot sustain. Stress components in a porous rock are (i) the mean stress acting on the solid, which is by definition the pressure the solid experiences (P_{solid} ; see Table 1 for a list of symbols), (ii) the deviatoric stress tensor, which is the stress tensor minus the solid pressure, and finally (iii) the pressure of the material inside the pores. Here we denote this material in pores with ‘fluid’, which can be air, gas, oil, liquid, such as an aqueous fluid, or magma. It is assumed that the viscosity of the fluid is so low compared to that of the solid that the differential stress (difference between maximum and minimum stress) in the fluid can usually be considered effectively zero. For a given porosity ϕ , the stress state of the rock $S_{ij}(\text{rock})$ can thus be described as the weighted average of the stress state of the solid $S_{ij}(\text{solid})$ and of the pore fluid, represented by the fluid pressure P_f :

$$S_{ij}(\text{rock}) = \phi P_f \delta_{ij} + (1 - \phi) S_{ij}(\text{solid}), \quad (1)$$

with δ_{ij} the Kronecker delta. The stresses and pressures are averaged over the volume of rock under consideration. Stresses inside the solid may vary especially strongly, for example at grain contacts

Table 1. List of symbols

Symbol	Unit	Description
a		Factor incorporating the effect of poroelasticity in Biot-type equations for effective stress
A	m ²	Area of a fracture
c	MPa	Cohesion
δ_{ij}	–	Kronecker delta
D	m ² s ⁻¹	Diffusion coefficient for fluid overpressure
E	MPa	Young’s modulus
ϕ	–	Porosity
g	m ² s ⁻¹	Gravitational acceleration
$f_{u/\sigma}(\theta)$		Geometrical factor for the displacement (u) and stress (σ) fields as a function of the angle θ relative to the long axis of a crack
G	N	Total force causing the growth of an extensional fracture
γ	J m ⁻²	Fracture surface energy
Γ	J	Total surface energy of a crack
ψ	°	Angle of internal friction
K	MPa	Bulk modulus
K_c	MPa	Fracture toughness
K_i	–	Stress intensity factor
L, L_c	m	Length of a fracture, critical length
λ	–	Pore fluid factor, i.e. the ratio of pore fluid pressure and vertical stress
m	–	Power-law exponent for size distribution of breccia clasts
μ	–	Coefficient of friction
ν	–	Poisson’s ratio
P_f	MPa	Fluid pressure
ΔP_f	MPa	Fluid overpressure: difference between fluid pressure and hydrostatic pressure
P_{hydro}	MPa	Hydrostatic fluid pressure
P_{rock}	MPa	Mean pressure in a volume of rock
P_{solid}	MPa	Mean pressure in the solid phase of a volume of rock
r	m	Radius of curvature of crack tip
$\rho_f, \rho_{\text{rock}}$	kg m ⁻³	Density of fluid and rock
$S (S_{ij})$	MPa	Total stress (tensor)
$\sigma (\sigma_{ij})$	MPa	Effective stress (tensor)
T	MPa	Tensional strength
τ	MPa	Shear stress
$U_{e/p/k}$	J	Elastic (e), plastic (p) or kinetic (k) energy
W	J	Work
z	m	Depth below the surface

or at the tips of microfractures. However, pressure in the fluid may also vary, especially when pores are not all connected well.

The ‘hydrostatic fluid pressure’ (P_{hydro}) is the fluid pressure in a fluid that is at rest and in contact with the Earth’s surface. P_{hydro} is the pressure caused by the weight of the water column. For a fluid with a mean density (angled brackets denote an average) $\langle\rho_f\rangle$, P_{hydro} at depth z is $\langle\rho_f\rangle gz$, with g the gravitational acceleration. In the same way, we can define the lithostatic pressure (P_{lith}), which is simply the pressure caused by the weight of the rock column with mean density $\langle\rho_{\text{rock}}\rangle$. For depth z we get $P_{\text{lith}} = \langle\rho_{\text{rock}}\rangle gz$. Fluid pressure can be above hydrostatic and is then often referred to as ‘overpressure’ (e.g. Osborne & Swarbrick, 1997). This may relate to the state of the absolute fluid pressure, for example when Sibson (2003) writes ‘overpressures may approach lithostatic values’. In this paper, we, however, prefer to define fluid overpressure (ΔP_f) as the difference between the actual fluid pressure and the hydrostatic fluid pressure: $\Delta P_f = P_f - P_{\text{hydro}}$. It should be noted that Gudmundsson (2011) and Phillip (2012) define overpressure as the total fluid pressure minus the normal stress on the fracture plane, which in the literature on fracture propagation is often called the ‘driving stress’, ‘driving pressure’ or the ‘net pressure’ (Spence & Turcotte, 1985; Rubin, 1995; Olson *et al.* 2009). While fluid overpressure is a scalar with an absolute value, it may sometimes be advantageous to use the fluid pressure relative to another reference pressure. Hubbert & Rubey (1959) introduced the ‘pore fluid factor’ (λ), which is the ratio of the pore fluid and the total vertical stress (also see Cox, 2010).

The fact that a reservoir can be stimulated by increasing the fluid pressure shows that the fluid pressure plays a role in fracture formation. Failure is thus not only a function of the absolute stresses, but effective stresses, which are the absolute stresses in relation to the fluid pressure. The simplest definition for ‘effective stress’ is the absolute stress minus the fluid pressure (Terzaghi, 1923). This definition is widely used in geology and we also use it in this paper, although will discuss below alternative definitions as well.

The term hydrofracture is commonly used as denoting fractures whose formation is induced by an elevated fluid pressure, as opposed to those formed by elevated differential stresses, typically because of tectonic stresses, but also due to, for example, meteorite impacts or igneous activity. For simplicity we group the latter fractures under the term ‘tectonic fractures’. While it may be clear that fractures are hydrofractures when they occur due to an artificial increase of the fluid pressure, it is not as simple to ascertain whether a natural fracture is due to an elevated fluid pressure (a hydrofracture), to elevated tectonic stresses (a tectonic fracture), or a combination of both, as is probably usually the case. For natural fractures we therefore here propose to refine the term ‘hydrofracture’ to mean *those fractures that are primarily caused by an elevated fluid pressure*. This definition does not exclude a contribution of tectonic stresses. What remains is to define ‘primarily’ as this now defines whether a fracture is a hydrofracture or not. We will address this issue further below.

By definition, cohesion is lost across a fracture surface. Over time, cohesion is usually recovered by healing, often by mineral precipitation in the space created in the fracture, i.e. the formation of a ‘vein’ (Bons *et al.* 2012; Laubach *et al.* 2019). However, space for mineral veins can also be created without fracturing, for example by dissolution. We therefore use the general definition by Bons *et al.* (2012) of veins as ‘mineral aggregates that precipitated from a fluid in dilational space, i.e., in space that was created in the rock’. This can be due to tensional failure, but is not restricted to this

process. If the space is filled with a frozen magma, it is called a dyke, inclined igneous sheet, or sill. While it is common for the space for veins to be created by a fracture, it is important to note that a vein is not necessarily a former fracture. In particular the controversial equation of fibrous or ‘beef’ veins with fractures will be discussed in this paper, as it has been used to argue for their origin as hydrofractures. Other examples of veins not forming by precipitation of minerals within fracture porosity are replacement veins (e.g. Fletcher & Merino, 2001; Pirajno, 2009).

3. Formation of hydrofractures

We divide the theory on hydrofractures in rocks into two topics: (1) the formation or nucleation of a new hydrofracture and (2) the propagation of an existing hydrofracture (Pollard & Aydin, 1988; Gudmundsson, 2011; Guerriero & Mazzoli, 2021). The difference is that for the first one we can usually assume a homogeneous stress and fluid-pressure state before the fracture forms. Once the fracture is formed, a complex stress field develops, particularly at the fracture tips (Engelder, 1999). Although the two processes are often treated separately, it is clear they are intimately linked as propagation can commence as soon as failure produces the first embryonic fracture. Nevertheless, here we follow the classical division and first deal with the initial formation of hydrofractures. We restrict ourselves to the basic Mohr–Coulomb–Griffith theory that does not take into account the interaction of chemical dissolution and precipitation reactions that intimately interact with a developing fracture or set of fractures, subcritical crack growth and ductile fractures, for which the reader is referred to Atkinson (1984), Weinberg & Regenauer-Lieb (2010) and the extensive review by Laubach *et al.* (2019).

3.a. Fluid pressure and initial fracture formation

An intact solid, such as a rock, will break or fail when the stress state reaches the failure criterion. The stress state can be described by the stress tensor (S_{ij}), or alternatively by the three principal stresses (S_1 , S_2 and S_3) in descending order of magnitude (with compressive stress taken positive here), and their orientations in space. Stresses can vary widely on the small scale (Pollard & Aydin, 1988). It is generally assumed that, at some scale above that of the homogeneous equivalent medium (HEM), the stress state can be described by a single stress tensor. The HEM scale is the scale well above smaller-scale heterogeneities, such as grains and pores in a sandstone, or stratigraphic layers in a basin. Whether failure occurs and, if it does, the orientation of the resulting fracture is entirely dependent on the stress state, the rock mechanical properties that are potentially anisotropic, and, if a pore fluid is present, the fluid pressure (P_f).

3.a.1. Mohr–Coulomb–Griffith theory for failure

Failure of rocks is conveniently analysed with the Mohr diagram for stress (Mohr, 1882) in combination with the Mohr–Coulomb–Griffith failure envelope (Terzaghi, 1943; Hubbert, 1951; Secor, 1965). An intact rock volume can be envisaged to contain an infinite number of potential fracture planes in terms of location and orientation, but the Mohr–Coulomb–Griffith failure theory is only concerned with the orientation of the plane or planes (with respect to that of the principal stresses) that will fail to form a fracture. In this theory, only the maximum and minimum principal stresses (S_1 and S_3) play a role and fractures form in a plane parallel to S_2 . The two-dimensional construction is thus for the

plane that contains S_1 and S_3 , and only considers potential fracture planes in the rock that are parallel to S_2 . The shear stress (τ) and normal stress (S_n) of a plane (parallel to S_2) that makes an angle α with the smallest principal stress (σ_3) are given by (Mohr, 1882; Hubbert, 1951; Fig. 1a):

$$\tau(\alpha) = (S_1 - S_3) \cdot \cos(\alpha) \sin(\alpha) = \frac{1}{2}(S_1 - S_3) \cdot \sin(2\alpha) \quad (2)$$

and

$$\begin{aligned} S_n(\alpha) &= S_1 \cdot \cos^2(\alpha) + S_3 \cdot \sin^2(\alpha) \\ &= \frac{1}{2}(S_1 + S_3) + \frac{1}{2}(S_1 - S_3) \cos(2\alpha) \end{aligned} \quad (3)$$

Equations (2) and (3) describe a circle in a plot of $\tau(\alpha)$ against $S_n(\alpha)$: the Mohr circle for stress (Fig. 1b). Each point on the circle represents the stress state for a plane with orientation α .

Within the τ - S_n space of the Mohr diagram there are τ - S_n conditions that a rock can sustain and those it cannot. This of course depends on the rock properties. The boundary between these two conditions is a line in the Mohr diagram: the failure envelope. A rock will fail as soon as a plane within the rock reaches a τ - S_n combination on the failure envelope. This means that the Mohr circle just touches the failure envelope and, therefore, that the slope of the failure envelope is parallel to the tangent of the circle at the point of contact. As a result, the slope of the failure envelope determines the orientation α of the plane of failure (Fig 1c).

The failure envelope is typically defined by two basic equations. Tensional failure occurs when the minimum stress (S_3) reaches the tensional strength (T). It is common in the literature to report the absolute (positive) value of the tensional strength, although the normal stress on the plane of failure is negative in case of tensional or mode-I failure. To avoid confusion regarding the sign, we here use the real, negative value of T for the tensional strength. The shear-failure criterion is defined by:

$$\tau = c + \mu \cdot S_n, \text{ or } \tau = c + \tan(\psi) \cdot S_n. \quad (4)$$

Here c is the cohesion, which is the shear stress acting on a fracture plane that experienced zero normal stress when it failed. A planar surface in a rock can typically sustain more shear stress as the normal stress on that surface increases. This is captured by the coefficient of friction (μ) or the slope of the failure envelope, defined by the angle of internal friction (ψ), typically in the order of 30–45°. It follows that $\mu = \tan(\psi)$.

Figure 1c shows the two basic types of failure: the first is shear failure resulting in a shear or mode-II fracture. It occurs when the Mohr circle touches the failure envelope for a plane that experiences a normal stress $S_n \geq 0$. Because of the symmetry of the stress state, the Mohr circle will reach the failure envelope twice in an isotropic rock. A conjugate set of fractures forms with opposite sense of shear. The resulting fractures, parallel to S_2 , make an angle of $\alpha = \pm(90^\circ + \psi)/2$ with S_3 . As ψ is usually positive, S_1 is in the bisector of the acute angle $90^\circ - \psi$ between the two fracture orientations (Anderson, 1905). A practical advantage of Anderson's theory of faulting (Anderson, 1905, 1951) is that this simple geometrical relationship between the stress field and shear fracture orientations allows revealing both the stress-field orientation and the angle of internal friction by measuring fracture orientations in the field. Gomez-Rivas *et al.* (2014), for example, used this to track the evolution of the orientation of the stress field in the

Jabal Akhdar Dome (Oman) from fault and vein orientations, first as a result of the emplacement and exhumation of the Semail Ophiolite and Hawasina nappes, and subsequently by the movement of the Indian plate relative to the Arabic plate. The second basic type is tensional failure, which occurs when the leftmost point on the Mohr circle is the first to reach the failure envelope. This means that failure occurs parallel to the plane normal to S_3 . Because this requires a negative normal stress, the resulting fracture is under tension and its two fracture surfaces can diverge: an open extensional or mode-I fracture forms (Fig. 1c).

Hybrid fractures form in the transition between the end members of extensional and shear fractures. Here the angle of internal friction decreases from 90° down to ψ for $S_n > 0$. One theoretical model for the failure criterion for hybrid failure was provided by Griffith (1924) for $S_n \leq 0$:

$$\tau^2 = \frac{c^2}{\tau^2} T(T - S_n), \text{ giving } \mu_{\text{hybrid}} = \frac{d\tau}{dS_n} = \frac{c}{2\sqrt{\tau^2 - S_n\tau}} \quad (5)$$

Note that the tensional strength (T) is negative here. The ratio of cohesion and tensional strength is not predefined in our Eq. (5). However, the ratio according to Griffith's theory c/T is -2 , therefore $c^2/T^2 = 4$ (Sibson, 2000a; Pollard and Fletcher, 2005; Jaeger *et al.* 2007; Gudmundsson 2011). Equation (5) implies that the hybrid angle of internal friction depends on the ratio of c and T . A problem is that this may lead to a discontinuity in ψ as S_n increases from negative to positive. With $c/T = -2$, the angle of internal friction is 45° at $\sigma_n = 0$ (Eq. 5), although angles of internal friction may vary widely for $\sigma_n \geq 0$ (Gudmundsson, 2011). Issues with the transition from hybrid failure to pure shear failure have been discussed by various authors (some examples are Secor, 1965; Phillips, 1972; Engelder, 1999; Ramsey & Chester, 2004; Zhu, 2017), but details of hybrid failure are not the main focus of this paper.

Although the Mohr–Coulomb–Griffith criterion has proven to be a very useful, or at least often employed, tool for the prediction of the onset of failure, as well as the type and orientation of resulting fractures, it cannot predict where a fracture would form, as the actual location where a fracture nucleates is controlled by the presence of flaws that perturb the local stress field (Pollard & Aydin, 1988). The Mohr–Coulomb–Griffith criterion does, however, include the presence of such flaws, as these affect the tensional strength, cohesion and angle of internal friction.

3.a.2. The effect of fluid pressure

So far, we have not considered how a pore fluid affects the stress state at which a rock fails. We have seen that with increasing confining pressure the Mohr circle required to reach failure shifts to the right and increases in size, and hence the required differential stress ($S_1 - S_3$) increases. This is because the confining pressure presses grains together, making it more difficult for them to separate and slide past each other. The basic failure envelope is thus essentially for a dry rock. The presence of a pore fluid with a pressure P_f modifies the stresses at grain contacts and will thus affect the point of failure. Rather than to account for this by adapting the failure envelope, the failure envelopes are kept as they are, and the concept of 'effective stress' is used. The effective stresses are calculated from the actual stresses and the fluid pressure in such a way that the rock with a pressurized pore fluid can be compared with the equivalent dry rock.

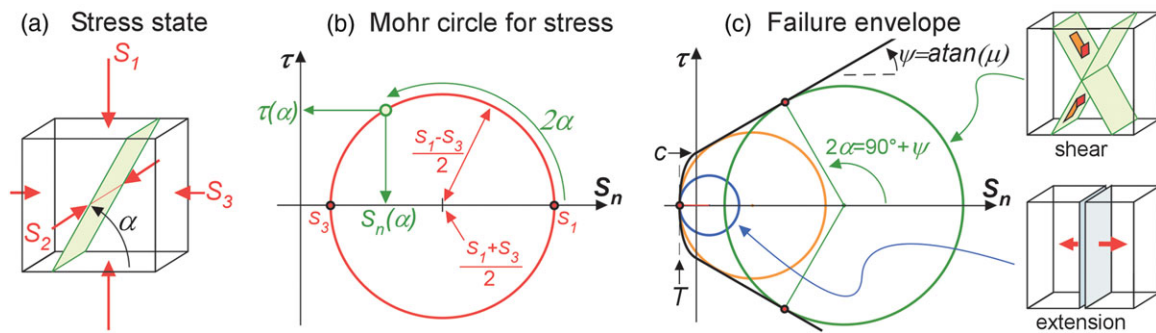


Fig. 1. Construction of the Mohr circle for stress. (a) Definition of the angle α between the minimum principal stress (S_3) and a plane parallel to the intermediate principal stress (S_2). (b) The Mohr circle for stress in a graph of τ versus S_n . The stress state for a plane with orientation α can be found by measuring an angle 2α from the S_1 point on the circle. (c) Mohr diagram with failure envelope, illustrating the two end-member failure types: shear failure and tensional failure. The orange circle is the circle that touches the failure envelope for both tensional and shear failure. Whether this can occur in a rock depends on the shape of the envelope at negative and low normal stress.

The simplest, and in geology most commonly used, way to determine the effective stresses (σ_{ij}) is by subtracting the fluid pressure from the actual stresses (S_{ij}), following the Terzaghi principle (Terzaghi, 1923):

$$\sigma_{ij} = S_{ij} - \delta_{ij}P_f \quad (6)$$

In the Mohr diagram this has the effect of shifting the Mohr circle to the left by the amount of P_f (Fig. 2a). When one keeps increasing the fluid pressure the rock will fail at some stage. The rationale is that the pore fluid carries part of the load applied to a rock and thus effectively reduces the stresses within the solid matrix. It should be noted that with the Terzaghi principle the size of the Mohr circle, and thus the differential stress, does not change as a function of P_f .

However, the Terzaghi principle is in some cases an oversimplification of the system and may lead to wrong interpretations, as discussed by many authors (e.g. Cleary & Wong, 1985; Meyer, 1986; Gordeyev & Zazovsky, 1992; Tzschichholz *et al.* 1994; Hillis, 2003; Cobbold & Rodrigues, 2007; Ghani *et al.* 2013; Koehn *et al.* 2020). The reason is that the Terzaghi principle essentially ignores that rocks are poroelastic, which means that both the pores and solid matrix, and therefore the bulk rock, change their volume if their pressures are changed. The basic theory for poroelasticity was developed for soils by Biot (1941, 1956) and elaborated on, or modified, by various others (see review by Guerriero & Mazzoli (2021), and references therein). Proposed equations for effective stress that take into account poroelasticity are mostly of the form:

$$\sigma_{ij} = S_{ij} - (1 - \alpha)\delta_{ij}P_f \quad (7)$$

As summarized in de Boer & Ehlers (1988, 1990) and Guerriero & Mazzoli (2021), a number of models for the parameter α have been proposed, such as α equals the porosity (Fillunger, 1936), $\alpha = K_{\text{rock}}/K_{\text{solid}}$ (for volume change with K the bulk modulus (Skempton, 1960; Nur & Byerlee, 1971)), or $\alpha = 1 - \nu/(1 - \nu)$ (with ν the Poisson's ratio; Hillis, 2003) that we discuss below.

Terzaghi's model is a special case with $\alpha = 0$ of the more general Biot model. This is the case when the solid matrix is rigid and load-bearing. Terzaghi's model with $\alpha = 0$ thus applies if the fluid overpressure is building up in a single pore, or in a restricted cell with overpressure in the crust. This is, however, often not even

approximately the case, especially in porous sediments that are far from incompressible and therefore have a Poisson's ratio of $\nu < 0.5$.

Boundary conditions become important when poroelasticity is relevant. If constant stresses on the boundaries are given, an increase in fluid overpressure will lead to a decrease in the principal effective stresses, but with a constant differential stress as was shown in numerical simulations (Koehn *et al.* 2020) and experiments (Cobbold & Rodrigues, 2007). This means that the size of the Mohr circle remains unchanged with a change in P_f and the Mohr circle shifts to the left or right according to Eq. (6). If, however, elastic strain is the boundary condition for the volume under consideration, things become more complicated as, for example, Hillis (2003), Cobbold & Rodrigues (2007) and Olson *et al.* (2009) point out. The reason is that a change in pore pressure requires a change in the applied stresses (S_{ij}) to maintain the given strain.

Hillis (2003) provided an example where a simple application of the Terzaghi principle does not work. The author examined an overpressure zone below a seal in a sedimentary basin and related the lowest effective stress below the seal to the vertical stress (S_v) and fluid pressure. The example considers a basin at rest so that it is neither extending nor shortening. The horizontal elastic strain is therefore zero ($\epsilon_h = 0$), while the vertical stress (S_v) on the rock is the overburden weight ($S_z = \langle \rho \rangle gz$). This is a case of mixed strain and stress boundary conditions.

If fluid pressure is zero (dry rock equivalent), the horizontal (S_h) and vertical (S_v) stresses are related by (using Hooke's law for linear elasticity and uniaxial strain and stress: $S_h = S_x = S_y$):

$$E\epsilon_h = S_h - \nu S_h - \nu S_z = 0 \Leftrightarrow S_h = \frac{\nu}{1 - \nu} S_z \quad (8)$$

In an incompressible rock ($\nu = 0.5$) this gives $S_h = S_v$, that is, zero differential stress. Although this would be correct for an incompressible rock, the resulting zero differential stress cannot simply be applied to a compressible rock. This would mean that the rock would compact equally in all directions and the basin would contract laterally. It is not permissible to use this stress state and simply subtract a non-zero fluid pressure to determine the effective stresses to assess potential failure or compaction. This is because total stresses change with increasing fluid pressure to maintain the boundary conditions. In an Andersonian stress state (Anderson, 1905, 1939) the vertical effective stress, resulting from a vertical stress boundary condition, does follow the straightforward Terzaghi model:

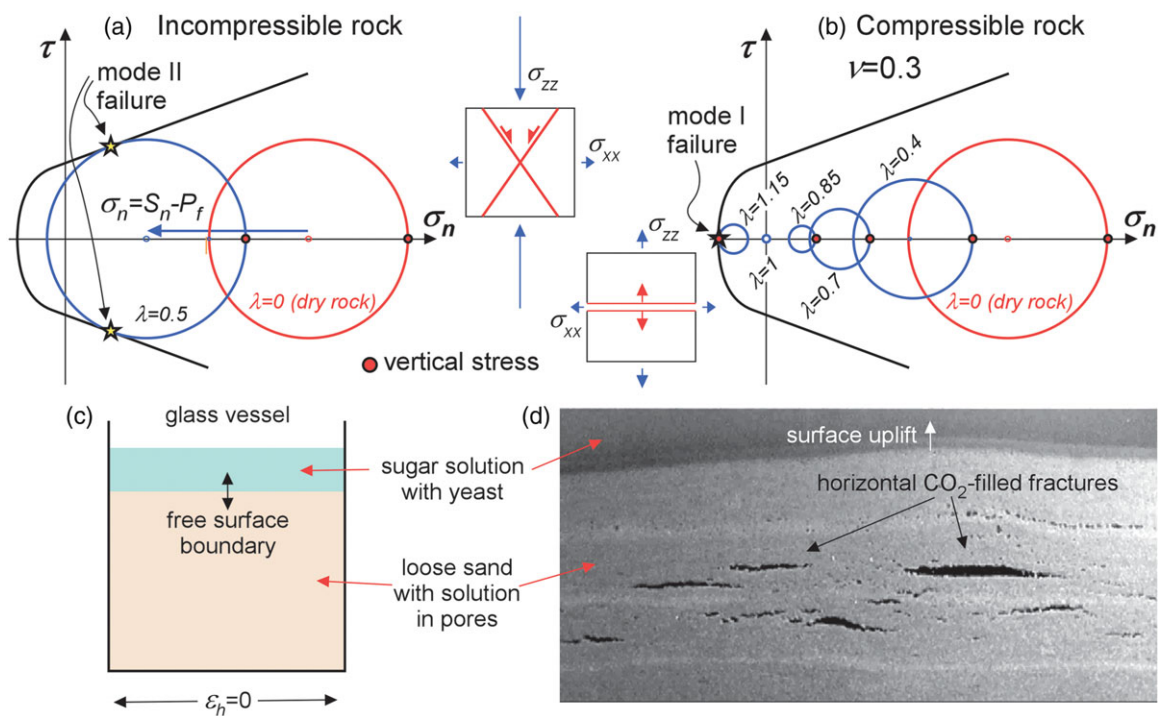


Fig. 2. (a) Terzaghi scenario for an incompressible material with the Mohr circle for the effective stress state moving by an amount of P_f towards the left-hand side without a change in differential stress. In the example with a vertical maximum stress (red dot), increasing the fluid pressure would eventually lead to shear failure. (b) Effect of compressibility in a situation where the vertical total stress is a function of the overburden load, and the horizontal stress is constrained by an imposed zero horizontal strain. Increasing the fluid pressure not only shifts the Mohr circle to the left, but also changes its size. Once fluid pressure exceeds the total vertical stress ($\lambda > 1$) the effective vertical stress (red dot) becomes the smallest stress and horizontal fractures form in case of failure. (c) Simple experiment illustrating the formation of horizontal extensional or mode-I fractures of Bons & van Milligen (2001). A glass vessel is filled with sand and water with dissolved sugar and yeast. Pressure of the fermentation product CO_2 increases until horizontal fractures form, as shown in (d).

$$\alpha_z = S_z - P_f, \text{ giving } \frac{d\sigma_z}{dP_f} = -1 \quad (9)$$

The horizontal effective stress, however, is a function of the zero horizontal strain boundary condition and the vertical fluid-pressure dependent effective stress, giving (Hillis, 2003; Cobbold & Rodrigues, 2007):

$$\sigma_h = \left(\frac{\nu}{1-\nu}\right)\sigma_z, \text{ giving } \frac{d\sigma_h}{dP_f} = \frac{-\nu}{1-\nu} \quad (10)$$

This means that with increasing P_f the vertical effective stress is reduced faster than the horizontal effective stress so that both will become zero when $S_z = P_f$ (Fig. 2b). Once the principal stresses reach negative values, the horizontal and vertical stress will become negative, where now the vertical stress is more negative and a horizontal fracture will develop upon failure (Cobbold & Rodrigues, 2007; Koehn *et al.* 2020). This can be illustrated with a very simple experiment (Bons & van Milligen, 2001) of a jar filled with loose sand and a pore fluid that initially consists of water, dissolved sugar and yeast (Fig. 2c). The glass walls of the jar provide zero horizontal strain boundary conditions. The top of the wet sand can move vertically, so here we have a stress boundary, with the total vertical stress increasing downwards according to the material density. Fermentation produces CO_2 gas that has a high wetting angle with the sugar solution. Permeability for CO_2 flow is therefore very low, as the gas tends to form bubbles in the pores and is inhibited from flow through the pore throats between the sand grains. The CO_2

pressure (P_f) increases as more and more CO_2 is produced, until finally horizontal mode I extensional fractures form (Fig. 2d). Gas generation in organic-rich shales and coals has been reported to induce natural hydrofractures (e.g. Fall *et al.* 2015).

The above should not be understood as taking sides in the discussion on whether Biot's or Terzaghi's theory (and derivations thereof) is right or preferred. Both are applicable depending on the rock properties and especially on the imposed boundary conditions. In the above case the vertical effective stress is $S_v - P_f$ (Eq. 8), which is according to Terzaghi's theory, but also Biot's theory with $a = 0$ (Eq. 7). Terzaghi's theory is also applied to calculate the effective horizontal stress as applied to Hooke's linear elasticity law (Eq. 8). The difference with the straightforward application of Terzaghi's principle is that, unlike the vertical stress, the total horizontal stress in this case is a function of the fluid pressure itself.

We have now seen that horizontal extensional fractures are expected to form in a basin at rest in which the fluid pressure is increased due to an influx of fluids from below (e.g. due to expulsion of compacting sediments, dehydration reactions, release of hydrocarbons). Typical fluid pressure profiles as a function of depth are shown in Figure 3. The presence of a low-permeability seal can locally bring the fluid pressure up to the failure condition (Fig. 3b) or in an overpressured layer, as modelled by Ghani *et al.* (2013, 2015) and Koehn *et al.* (2020) (Fig. 4a,b). A tacit assumption so far was that there are no lateral gradients in fluid pressure. If these gradients exist, for example in laterally constrained high-pressure cells, the zero horizontal strain condition does not apply

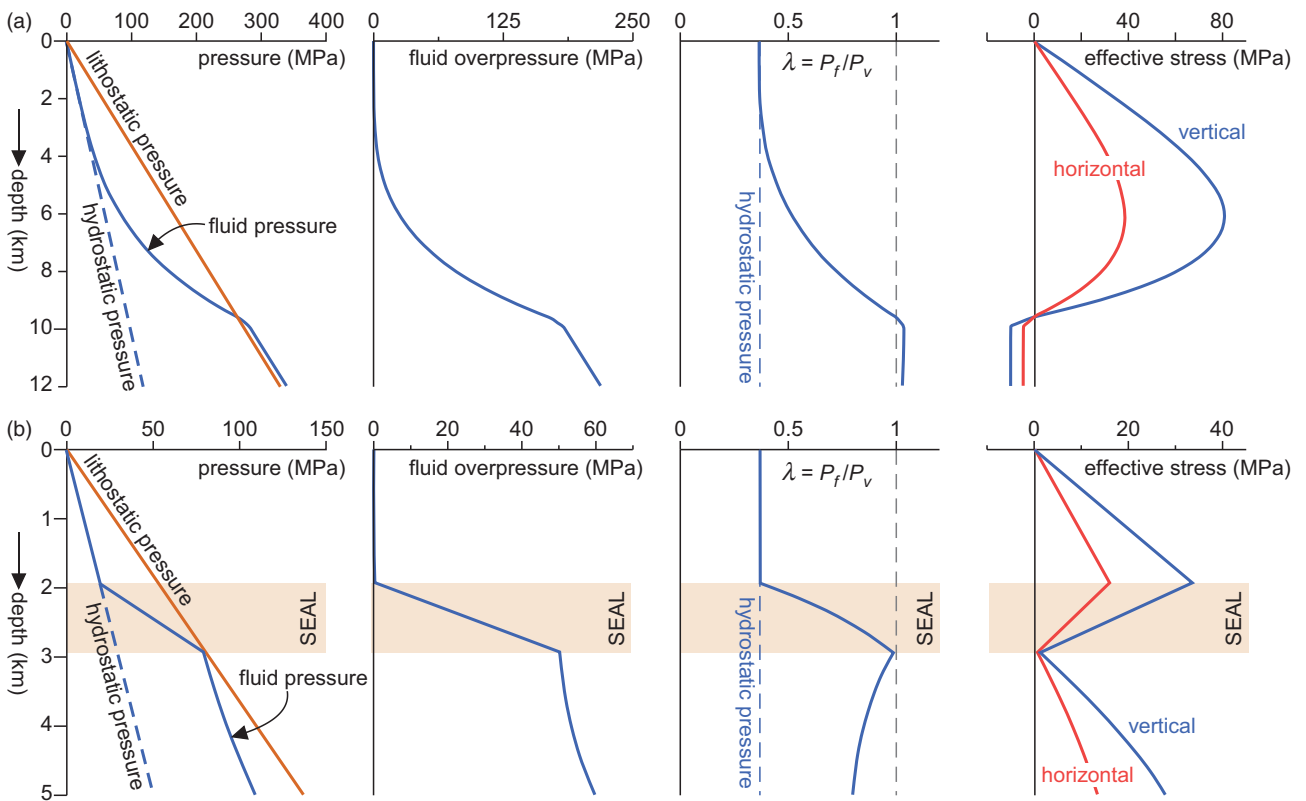


Fig. 3. Depth profiles for a fluid influx of $5 \times 10^{-11} \text{ m s}^{-1}$ from below and a permeability that decreases with depth according to Ingebritsen & Manning (1999), (a) without and (b) with a low-permeability seal. From left to right, we show absolute pressures, the fluid overpressure, the pore-fluid factor (λ) and finally the effective stresses for a basin at rest and a Poisson's ratio of 0.4.

anymore and the simulations in Figure 4c–e show that an increase in fluid pressure leads to fractures in different orientations, and potentially shear fractures as well.

3.b. Beyond the initial fracture development

3.b.1. Fracture propagation and stress intensity factor

We now look at the propagation of simple cracks using linear elastic fracture mechanics and the idea that crack propagation costs energy because new surface area is created (Griffith, 1920). In order to conserve energy, the work per unit time of an applied load is equal to the rates of change in elastic (\dot{U}_E), plastic (\dot{U}_P) and kinetic energy (\dot{U}_k), as well as the energy per unit time spent to increase the crack area ($\dot{\Gamma}$) (Griffith, 1920; Richard & Sander, 2016):

$$\dot{W} = \dot{U}_E + \dot{U}_P + \dot{U}_k + \dot{\Gamma} \tag{11}$$

If we assume that the crack propagation is slow, then the kinetic energy can be neglected. With this the rate of change of potential energy of the system as a function of crack surface area change, i.e. crack growth, can be calculated.

For a simple extensional crack in an extensional system that is purely elastic this formulation leads to the Griffith criterion for extensional cracks where G , the crack extension force, is proportional to changes in elastic and surface area according to (Griffith, 1920; Richard & Sander 2016):

$$G = \frac{\partial U_E}{\partial A} \tag{12}$$

Using the stress solutions by Inglis (1913), Griffith (1920) derived a strength criterion that can be used to estimate at what stress (T) a material will fail:

$$T = \sqrt{\frac{E\gamma r}{4lL}} \tag{13}$$

with E the elastic modulus, γ the surface-free energy, r the radius of curvature of the crack tip, l the bond length of the material and L the crack length. It is worth noting that the original Griffith formulation was derived for a crack with internal stress on the walls, which is the same as an external extensional load on an infinite plate. Therefore, the simplest hydrofracture is an extensional fracture, where the internal fluid pressure is equivalent to an external negative stress on the medium. Of course, once the fracture propagates and opens, changes in the fluid pressure as well as geometrical changes of the crack have to be taken into account.

For certain scenarios the stress, strain and displacement fields for a crack propagation in an elastic medium can be solved analytically (Westergaard, 1939). This leads to the following expressions for the state of stress

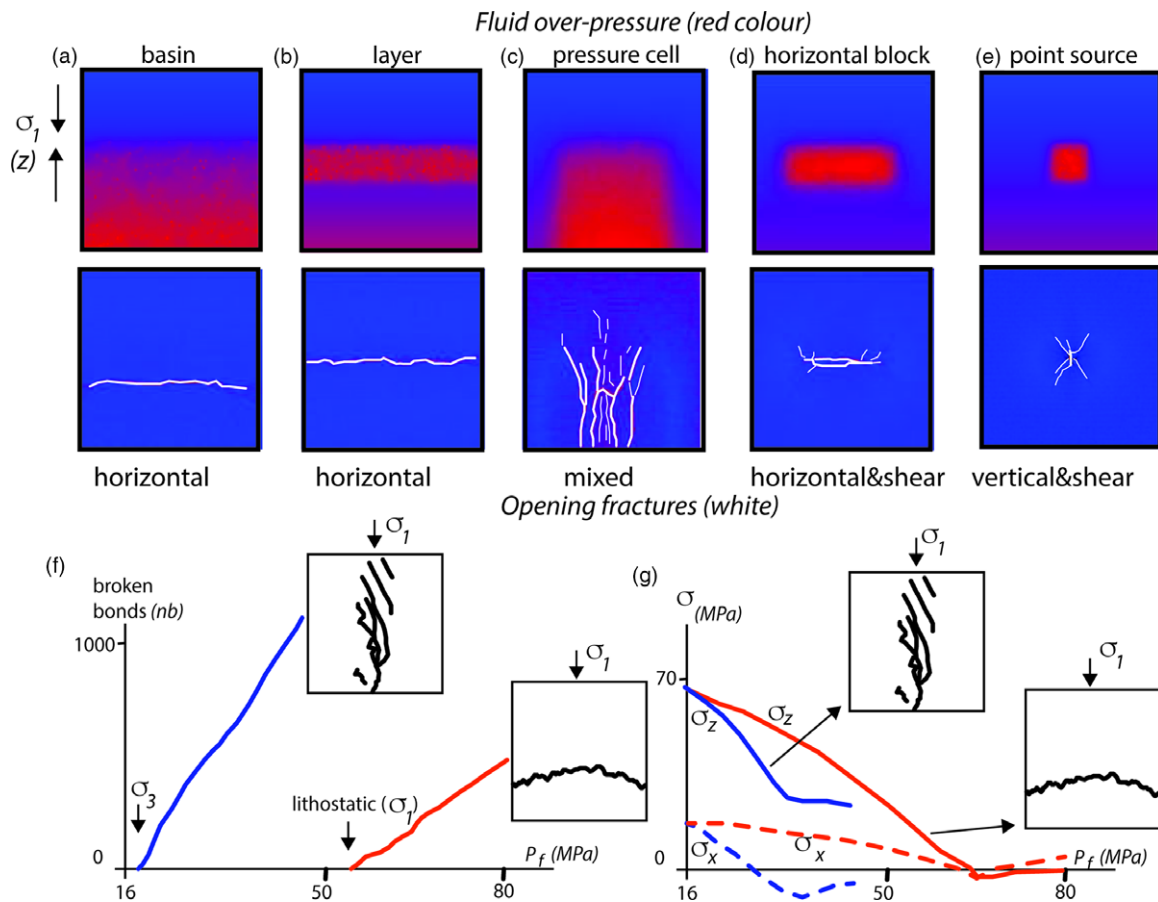


Fig. 4. Variations of the geometry of a high fluid pressure zone in simulations leading to a variety of fracture patterns from horizontal to vertical as well as combinations. (a–e) upper pictures show fluid pressure in the model with red high and blue low pressure. (a–e) lower pictures show the developing opening fracture patterns for the specific cases in the models in white. (a) and (b) are cases where the boundaries are fixed, and fluid pressure builds up in a sedimentary basin or a horizontal layer and the resulting fracture is horizontal. (c–e) show a variation of localized high fluid pressure cells where fracturing can happen in a vertical and horizontal orientation. (f) shows the developing fractures as a function of fluid pressure for two end-member cases representing (a) a sedimentary basin with fixed boundaries in blue, and (c) a fluid pressure cell that represents a horizontal stress boundary in red. The corresponding solid stresses as a function of the fluid pressure are shown in (g) for both cases. Note that fractures develop early in case (c) and the evolving stress field follows Terzaghi’s law (blue curves). In case (a), represented by the red curves, differential and mean stress decay and fracturing happens at a much higher fluid pressure.

$$\sigma_{ij} = \frac{K_i}{\sqrt{2\pi r}} f_{ij}(\theta) \tag{14}$$

and displacement

$$u_{ij} = \frac{K_i}{2\mu} \sqrt{\frac{r}{2\pi}} g(\theta) \tag{15}$$

with K the stress-intensity factors that contain loading as well as geometrical conditions, r the distance to the crack tip, and $f_{ij}(\theta)$ and $g(\theta)$ functions of the angle θ relative to the long axis of the crack (Sih, 1973; Rooke & Cartwright, 1976). Theoretically these formulations only work away from the actual crack tip, while at the tip (at $r=0$) stresses form a singularity-dominated zone. The stress intensity factor varies for crack types such as extension versus shear as well as boundary conditions and crack geometries. For a simple hydrofracture in terms of the Griffith extensional crack we have:

$$K_i = \sigma \sqrt{\pi L} \tag{16}$$

A geometrical factor needs to be added for more complex configurations. For constant geometries several known stress intensity factors can be added (Sih, 1973; Rooke & Cartwright, 1976), which essentially leads to the Terzaghi criterion where stresses due to an internal fluid pressure cancel out stresses from an external loading, which leads to the idea of an ‘effective stress’. The superposition of stress intensity factors for variable stress fields known from literature offers advanced approaches extending the Mohr–Coulomb approaches, discussed above, to study hydrofractures that develop under variable boundary conditions in the Earth’s crust.

For more complicated fracture propagation problems, stress intensity factors can be determined in continuum simulations to calculate the most probable path of propagation and then re-mesh the model. Another possibility is the use of discrete element models where bonds with a critical breaking threshold break as will be discussed in the following.

3.b.2. Growth of individual fractures and fracture and vein networks

Hydrofractures in general are introduced into the system because there is an overpressure as a result of the difference between the

surrounding fluid pressure and a zone where fluid pressure is elevated. The overpressure (ΔP) is a function of the local increase in pressure as a function of time and the advection of the overpressured fluid away from the zone of influx or fluid production. How much the fluid leaks into the system depends on the permeability of the host rock. If the fluid addition is faster than the leaking or if the rock is very impermeable the overpressure builds up until failure occurs. The creation of hydrofractures will now generate a higher permeability. The hydrofractures will grow until they have created enough permeability for the overpressure to dissipate into the rock at a given fluid addition rate. This is shown in a simulation in Figure 5 where the fluid overpressure at one point increases until a fracture network develops that drains the incoming fluid (for the numerical method see the Supplementary Material available online at <https://doi.org/10.1017/S0016756822001042>). The rock dynamically creates the permeability it needs to be able to drain the injected fluid.

A similar situation to that of the injected fluid case can be envisioned in a scenario at geological timescales. When the system is too permeable the fluid overpressure will never build up to be high enough to cause rock failure. However, if a seal exists or the rock itself is impermeable (Fig. 3b), an increase in fluid overpressure may lead to fracturing. This increase can happen, for example, during exhumation, thermal expansion of fluids, a de-watering reaction, oil maturation or release of fluids from a subducting slab, among other processes. Once fractures form, they may in turn lead to an increase in permeability and leaking of the overpressure. If the pressure is not released the fracture pattern may evolve dynamically. This is illustrated in Figure 5 where fractures develop below a seal in a simulation. Here the initial fractures follow Terzaghi's principle and are vertical and parallel to the largest principal stress (in this case vertical because of gravity). However, with increasing fluid pressure the pattern changes and the fluid pressure gradients work upwards and lead to the formation of an increasing number of horizontal fractures. The developing network is similar to a hydraulic breccia and forms because the seal is not broken. The final fracture network does contain fractures that formed in rather different stress fields. In a natural setting one may not be able to separate the different fractures from each other, making it hard to interpret the fracture network.

The system becomes even more complex when the fractures heal and form veins. It is important to note that veins are not equal to fractures, meaning that (a) the geometry of a vein does not necessarily reflect that of the original fracture, (b) not all veins represent fractures (e.g. in the case of replacement veins, veins filling dissolution vugs or fibrous veins; see below), (c) not all veins represent fractures that open at the same time (such as in the case of crack-seal veins; Bons *et al.* 2012; Virgo *et al.* 2014), (d) veins may refracture several times (Ramsay, 1980) and (e) veins may change the properties of the system. An example is given in Figure 6 in a simulation following the general set-up of Ghani *et al.* (2013)). The fractures develop due to fluid overpressure build-up below a seal (in blue colour). In these simulations, the fractures can heal following the algorithm of Vass *et al.* (2014) and once they heal the new bonds can have different properties. New veins either fracture more easily (weak in Fig. 6) or are more difficult to fracture (strong in Fig. 6) than the host rock. The properties of the veins change the system completely and influence the development of new fractures. The two pictures on the left-hand side in Figure 6 show the open fractures at a given time step, and the picture on the right-hand side the vein network. One can see that the vein network and the fracture network are very different and that they vary

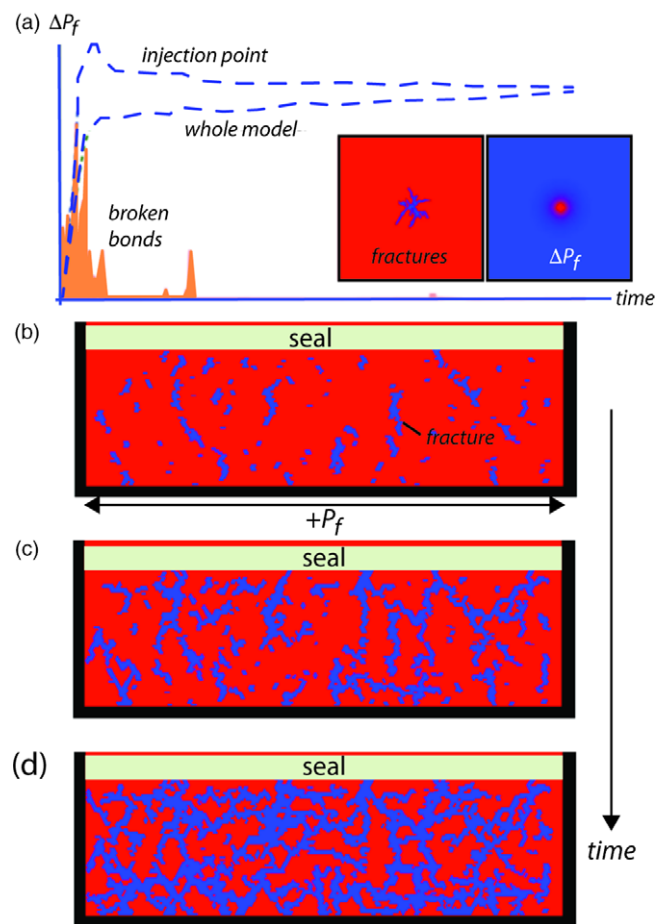


Fig. 5. (a) Injection of fluid and associated fracturing in a simulation (Ghani *et al.* 2013; Koehn *et al.* 2020). The two dotted curves show the fluid pressure evolution over time, one directly at the centre and one for the whole model. The developing fractures are shown in pink, the inset on the left-hand side shows the fracture pattern in blue and the inset on the right-hand side the fluid pressure (red high, blue low). (b–d) Simulations of the development of a fracture network below a seal at the top of the model as a function of an increase in fluid overpressure. The number of fractures, shown in blue, increases with model time and fluid pressure. Vertical stress is highest due to gravity, and horizontal stress is a function of the vertical stress. Box walls at the bottom and the right- and left-hand side are fixed.

significantly as a function of the failure properties of the veins. The weak veins have a memory and continue to open, leading to a large connected fracture network that breaks the seal. The hard veins produce a system with a large number of veins that do not refracture, while the material hardens and only a small number of open fractures remain. The important message is that we need to be extremely careful to relate vein networks directly to networks of active or open fractures. In the case of Figure 6, a large vein network means very few actually open fractures, because the system clogs itself. The relevance of this issue is illustrated with the discussion on how melt is extracted from partially molten rocks towards dykes that feed plutons and magma chambers. Marchildon & Brown (2003) used outcrops of networks of granitic dykes as evidence for magma transport through hydrofracture networks in support of the 'rivulets-feeding-rivers' model. Bons *et al.* (2009), however, argued that these networks are the cumulative product of many individual hydrofracture events, whereby new hydrofractures cut already fully solidified dykes. As such, there never was a fully percolating network of hydrofractures that were all filled with liquid

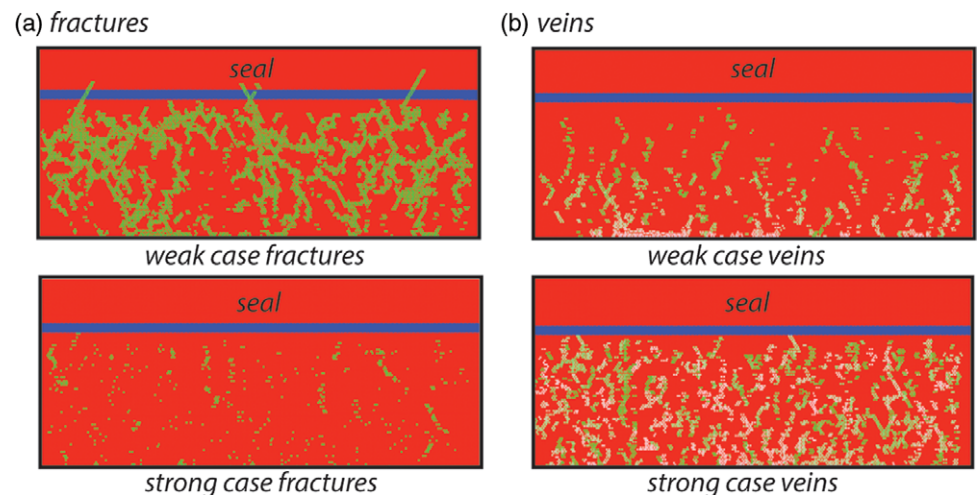


Fig. 6. Healing of fractures and the creation of veins with different breaking strength. Fractures in (a) in green colour and veins in (b) in green (early veins) and white (late veins). Weak veins that fracture more easily than the host rock are shown in the upper pictures, and hard veins that fracture less easily than the host rock in the lower pictures (see also Vass *et al.* 2014). Fluid pressure injected below a seal as in Figure 4 b-d over the whole width of the model.

magma, which the authors used as an argument against the ‘rivulets-feeding-rivers’ model.

3.b.3. Compressible fluids and hydromechanical interactions

Although not always considered, fluid compressibility is an important factor (e.g. Engelder & Lacazette, 1990). The compressibility of aqueous fluids typically is one order of magnitude lower than that of solids (e.g. Gibiansky & Torquato, 1998). In order to understand the interaction between fluid and solid after a hydrofracture network developed, one needs to take the compressibility of both media into account. The resulting structures form fracture channels of high porosity and compacted areas that dynamically open and close. This can be observed in numerical models (Fig. 7), as well as in experiments with granular media and injecting fluids or air, which in fact is also a fluid (Flekkøy, 2002; Johnsen *et al.* 2006, 2008a, b; Vinningland *et al.* 2007a, b, 2010, 2012; Goren *et al.* 2010, 2011; Niebling *et al.* 2010a, b; Ghani *et al.* 2013, 2015; Aleksans *et al.* 2020; Koehn *et al.* 2020). In the numerical model the fractures are first created and are then followed by the development of fracture channels that form as connected fractures that can open while the surroundings are compacted and thus closed. This dynamic system can lead to characteristic length scales in the model between sets of opening fracture channels that can be observed in experiments and may also be present in real systems.

3.b.4. Wholesale propagation of hydrofractures

Fluids in a fracture usually have a lower density than the surrounding wall rock. In the case of aqueous fluids this difference can be significant. The resulting buoyancy of the fluid can lead to unidirectional, upwards propagation at the upper tip of a fluid-filled fracture. Igneous dykes emanating from a magma chamber have a contiguous source volume that can feed the dyke for a prolonged period of time (Secor & Pollard, 1975; Clemens & Mawer, 1992; Rubin, 1995; Gudmundsson, 2011). However, when the fracture is sourced from a partially molten region or is filled with an aqueous fluid a large single feeder volume is usually absent and influx of fluid into the fracture may not keep up with the increasing fracture volume (Bons *et al.* 2009). In that case the fracture would begin to close at its bottom end (Bons *et al.* 2001; Rivalta *et al.* 2015). Weertman (1971) first proposed that if a fracture that is filled with a buoyant fluid is tall enough, it may keep propagating at its upper end, while closing at its bottom end. As a result, the fracture propagates together with its contained fluid. Such hydrofractures have

been called ‘Weertman (–Nunn) fractures’ (Rivalta *et al.* 2015) or ‘mobile hydrofractures’ (Bons, 2001). The basic theory was further developed by e.g. Secor & Pollard (1975), Pollard (1976), Nunn (1996), Dahm (2000) and Dahm *et al.* (2010) and extensively reviewed by Rivalta *et al.* (2015). Takada (1990), Dahm (2000), Bons (2001), Bons *et al.* (2001) and Rivalta *et al.* (2005) published analogue experiments of the ascent of mobile hydrofractures.

A non-horizontal fracture experiences a normal pressure gradient as the pressure in the wall rock increases faster with depth than inside the fracture that is filled with a lower-density fluid (Fig. 8). Fluid pressure inside the fracture and elastic strain of the wall rock adapt such that the fluid exceeds the pressure of the wall rock at the upper tip, the amount of which increases with the fracture length L . At a certain length the stress intensity at the upper tip reaches the fracture toughness, K_c , at which point the fracture will start to propagate upwards, while it closes at the base. The critical length, L_c , is given by Dahm (2000):

$$L_c = 2 \left(\frac{K_c}{\sqrt{\pi} g (\rho_{rock} - \rho_f)} \right)^{\frac{2}{3}} \quad (17)$$

The vertical critical length may range from as low as a few metres for a water-filled fracture to kilometres for dykes in the mantle, depending on the density difference between the rock and the fluid, and the poorly constrained fracture toughness, for which estimates range from $<1 \text{ MPa m}^{1/2}$ to a few $\text{GPa m}^{1/2}$ (see discussion in Dahm, 2000). Once a fracture becomes unstable and starts propagating, its velocity is controlled by the viscous drag of the contained fluid that has to flow upwards in the narrow fracture, as well as the fracture toughness at the propagating upper tip. Theoretical estimates for the ascent rate of critical-length mobile hydrofractures range from $< \text{m/yr}$ to $> \text{m/s}$ (Spence & Turcotte, 1985; Nunn, 1996; Dahm, 2000). Velocities up to m s^{-1} have also been inferred from lifting by the fluid of clasts and mineral fragments in veins and breccias (Oliver *et al.* 2006b; Okamoto & Tsuchiya, 2009; Weisheit *et al.* 2013a). The critical length is the length at which instability is reached, and the ascending fracture may get arrested as soon as conditions change. However, channelling along structures, such as faults or pathways of earlier mobile hydrofractures, may lead to the accumulation of multiple fluid batches to create more voluminous and faster mobile

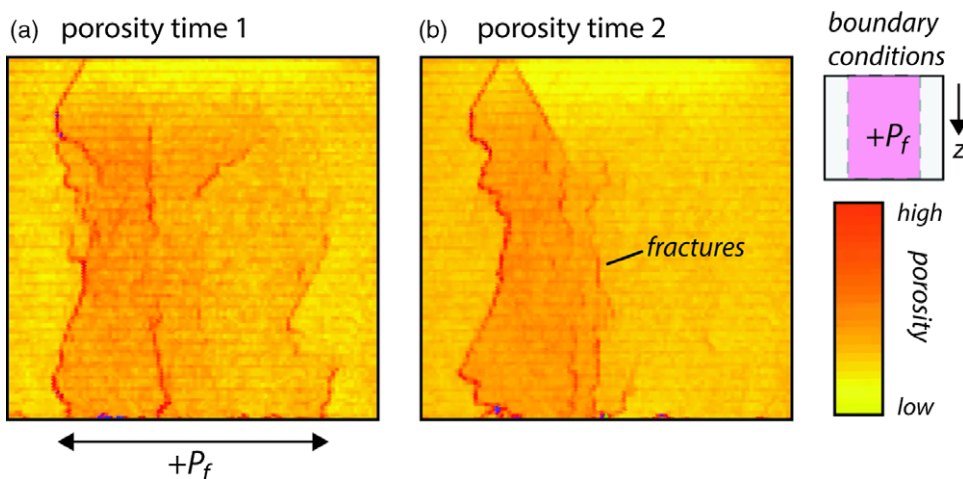


Fig. 7. Opening fracture channels that develop in a numerical model with a compressible fluid and full hydrodynamic interactions (see also Koehn *et al.* 2020). Colours are porosity with yellow low and red high porosities. Gravity is applied vertically and increase in fluid pressure is concentrated within the centre of the model. Large vertical fracture channels develop that drain the fluid and open and close dynamically.



Fig. 8. (a) Fluid pressure in a vertical open fracture in relation to lithostatic pressure that acts as a normal stress on the fracture, plotted as a function of depth. (b) Giant quartz vein from Poolamacca Station, far-west New South Wales, Australia, attributed by Bons (2001) to fluid transport by mobile hydrofractures. (c) Similar giant quartz vein northeast of the town of Roses, far-eastern Pyrenees, Spain.

hydrofractures that can ascend far up the crust (Maaløe, 1987; Sleep, 1988; Bons, 2001).

A problem with mobile hydrofractures is that, due to their very nature of being mobile, one cannot find these in their mobile state in the fossil record. Indications for active ascent of hydrofractures can be derived from rising microseismicity fronts (Dahm *et al.* 2010) or pulsed discharge rates of oil in mud volcanoes in the Gulf of Mexico (MacDonald *et al.* 2000). The fossil record can only provide indirect indications of fluid transport by mobile hydrofractures.

Mobile hydrofractures can theoretically transport batches of fluid upward very rapidly. At 0.1 m s^{-1} , a batch of fluid can ascend 10 km in about a day. This means that the fluid may not have time to equilibrate with the rapidly changing ambient conditions, except for adiabatic cooling, and can carry its dissolved mineral content up the crust to where the mobile hydrofracture is finally arrested. According to Bons (2001), this transport mechanism may explain the occurrence of huge quartz veins at Poolamacca station in far west New South Wales, Australia (individual vein volume up to an estimated $5 \times 10^5 \text{ m}^3$) (Fig. 8b), and also be found throughout the world, in, for example, the Pyrenees (Fig. 8c; González-Esvertit *et al.* 2022), the Sperrin Mountains of northern Ireland (Rice *et al.* 2016), the Bavarian Pfahl zone of the Bohemian Massif (Schaarschmidt *et al.* 2019), the Monte Rosa area in the

Western Alps (Pettko & Diamond, 1996), the Bundelkhand craton in the central Indian shield (Pati *et al.* 2007) or the Alaskan Cordillera (Goldfarb *et al.* 1993). However, other authors have also invoked different mechanisms for the formation of large quartz veins based on structural and geochemical arguments (e.g. Sharp *et al.* 2005), and thus the origin and significance of these impressive structures still raises questions.

Although the theory of mobile hydrofractures was originally based on water-filled crevasses in glaciers (Weertman, 1971), it is mostly applied to magma transport in dykes, where it remains controversial. In particular Lister & Kerr (1990, 1991) and Petford *et al.* (1993) objected that it is (i) theoretically impossible to completely close a fracture at the rear end if the contained fluid has a non-zero viscosity and that the fracture would thus lose fluid, and (ii) that a fracture that is just at its critical length L_c would still be so narrow that it would freeze quickly as it ascends into cooler crustal levels. The first point was addressed by Bons *et al.* (2001), who emphasized that initial critical-length mobile hydrofractures may get stalled and then merge with subsequently arriving hydrofractures, to form mobile hydrofractures that are well beyond the critical length L_c . The second point only applies to igneous fluids that can freeze. However, tall igneous dykes do exist, which is consistent with the fact that such dykes may tap large magma reservoirs that allow continuous feeding of a dyke and avoid

pinching off to form isolated ascending magma batches. This is also related to the viscosity of the fluid, which is generally much higher for magmas than for aqueous or hydrocarbon fluids, as is comprehensively discussed in Rivalta *et al.* (2015).

3.b.5. Dynamics of crustal-scale flow in hydrofractures

Hydraulic breccias (Jébrak, 1997; Weisheit *et al.* 2013a) and crack-seal veins (Ramsay, 1980) indicate stress states that frequently reach the failure criterion, and in some cases fast and localized fluid flow. In fact, many authors identified episodic pulses of rapid fluid flow (Sibson *et al.* 1975, 1988; Hunt, 1990; Nakashima, 1993; Cartwright, 1994; Cox, 1995; Eichhubl, 2000; Cox, 2005; Okamoto & Tsuchiya, 2009). It is worth noting that crack-sealing by itself is not necessarily evidence for rapid fluid flow (Becker *et al.* 2010). However, Darcian flow (e.g. Bear, 1988) is often used in crustal-scale fluid flow models, where fluid is assumed to flow continuously and slowly through pore space, driven by, for example, topography differences (Oliver, 1986; Oliver *et al.* 2006a; Person *et al.* 2007) or fluid density gradients associated with thermal instabilities (Matthäi *et al.* 2004; Zhao *et al.* 2008). When hydraulic head gradients are low, Darcian porous flow can be described as 'diffusional', because the fluid overpressure evolves in a diffusional way according to a diffusion coefficient related to the permeability. When the rock's permeability is insufficient to drain the fluid, fluid pressure builds up until the failure threshold is reached, thus activating hydrofractures. Open fractures suddenly increase the local permeability, and therefore fluid drainage, or can rapidly propagate together with their contained batch of fluid as mobile hydrofractures (Bons, 2001). These very rapid fluid-flow modes can be termed 'ballistic' (Bons & van Milligen, 2001).

Permeability, as one of the main controls on fluid flux, varies from 10^{-7} m² in well-sorted gravels to $< 10^{-23}$ m² in some crystalline rocks. It generally decreases logarithmically with depth (Ingebritsen & Manning, 1999; Manning & Ingebritsen, 1999; Cox, 2005). In the Earth's crust, permeability changes due to a variety of processes, such as compaction and decompaction, fluid flow and fluid production (e.g. dehydration reaction, fluid release by crystallizing magma), tectonism, and seismicity (e.g. Sibson *et al.* 1975; Walder & Nur, 1984; Yardley, 1986; Nor & Walder, 1992; Connolly, 1997; Cox, 2005; Hooker & Fisher, 2021), and has therefore been described as a dynamically self-adjusting property (Townend & Zoback, 2000; Rojstaczer *et al.* 2008; Ghani *et al.* 2015; Weis, 2015; Koehn *et al.* 2020; Fig. 5). As permeability can change suddenly over many orders of magnitude, Miller and Nur (2000) described the self-adjustment as a toggle switch that can lead to intermittency and self-organization (Sibson *et al.* 1988; Sibson, 2000a, b; Cox, 2005; Weis, 2015; Preisig *et al.* 2016).

Dynamic fluid transport has been numerically modelled with cellular automata in several studies (Miller & Nur, 2000; Bons and van Milligen, 2001; de Riese *et al.* 2020; Hooker & Fisher, 2021; Wangen, 2022). Miller and Nur (2000) and Bons and van Milligen (2001) both showed that fluid flow self-organizes as soon as a critical state is reached, which activates hydrofracture-controlled fluid flow as a ballistic fluid transport mode, resulting in power-law distributed frequencies of hydrofracture sizes. Wangen (2022) utilized the same approach to model fluid expulsion from compacting sediments. In reality, transport of fluid through the crust is never exclusively diffusive Darcian, or intermittent hydrofracture flow only, but rather a combination of the two end members (e.g. Shapiro & Dinske, 2009). The interaction between these two end members of fluid flow was investigated in detail in de Riese *et al.* (2020), and the resulting patterns are shown

in Figures 9 and 10. A description of the model is given in the Supplementary Material (available online at <https://doi.org/10.1017/S0016756822001042>). The model box (Fig. 9a, b) illustrates a 10 km tall vertical section through the Earth's crust, with a constant fluid flux entering at the base of the model that is characteristic for crustal metamorphic fluid fluxes at a depth of *c.* 10–15 km (Ingebritsen & Manning, 1999). The model only considers overpressure, which diffuses to simulate porous flow through the rock matrix. The effective pressure diffusion coefficient, *D* (see Supplementary Material), is varied, which implies a variation in permeability, and allows investigating the interaction of hydrofracture- and Darcian-dominated fluid flow.

Fluid production induces increasing fluid pressures, depending on the fluid overpressure diffusivity *D* (Fig. 9a). As soon as fluid pressure reaches the failure criterion (lithostatic pressure), a hydrofracture develops in the model. It can subsequently propagate depending on the fluid overpressure in its vicinity. At a very high permeability relative to the fluid flux ($D = 10^{-4}$) almost all fluid overpressure is dissipated by diffusional matrix flow towards the top of the model. In case of zero permeability ($D = 0$) all fluid transport takes place by hydrofracture propagation only. Hydrofractures that reach the top of the model domain drain all the fluid they contain, which effectively means the fluid overpressure is set to zero in that hydrofracture. Figure 9b shows the pressure field evolution with time of a simulation with $D = 2 \times 10^{-6}$ where both transport modes are active. Drainage of large hydrofractures results in low fluid overpressures in the top half of the model. The pressure field shows how the sharp boundaries of a hydrofracture become fuzzy with time as fluid flows in or out of the fracture after its arrest or drainage out of the top of the model. The mean pressure versus time in the system is shown in Figure 9c. In the case of pure hydrofracture flow the fluid pressure fluctuates strongly, although the input flux is constant. With increasing *D*, pressure fluctuations start to become periodical, while hydrofracture events become less frequent. When permeability is very high ($D = 10^{-4}$) the mean pressure becomes highly periodical, as fluid pressure can simultaneously build up in the whole model until a single very large hydrofracture discharges all the fluid and the fluid overpressure is reset to a low value throughout.

Sizes of hydrofractures that do not reach the surface have a power-law distribution (Fig. 10). Hydrofractures that can reach the surface have frequency size distributions that do not follow a power law. These hydrofractures are always large and scarce. With an increasing diffusion coefficient *D*, the hydrofracture frequency decreases, especially the frequency of hydrofractures that do not reach the surface (Fig. 10). Meanwhile, the size and fraction of fractures reaching the surface increases. Hydrofractures that are not able to reach the surface are constrained to the bottom part of the model, just above the fluid source. They spread the fluid within the crust. Their power-law distributions show that large but rare events transport most of the fluid, and indicate self-organized criticality (SOC) in the transport dynamics (Bak *et al.* 1988; Turcotte, 1999). Self-organization develops due to the existence of a failure threshold, which leads to the activation of a ballistic transport mode and the discharge of the excess fluid as soon as the failure threshold is locally overcome.

Hydrofractures reaching the surface of the model domain transport the entire fluid volume with few but large events (Fig. 10). These large events can be called 'dragon kings' (Sornette, 2009), which are outliers coexisting with power-law distributions, but taking on very high values far beyond those of the power-law distribution. They are usually associated with the

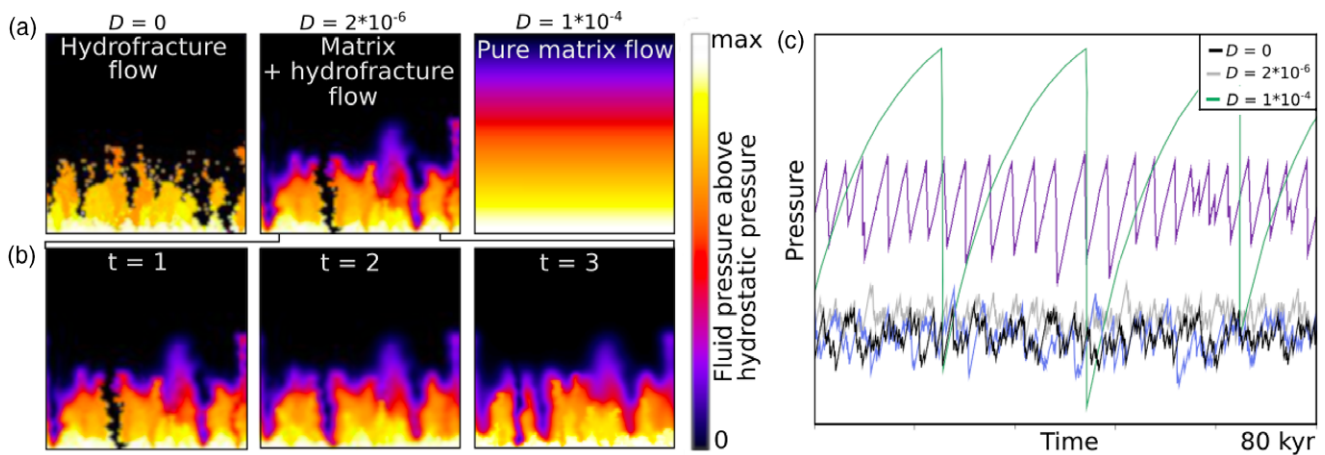


Fig. 9. Modelling results showing behaviour of hydrofracture and Darcian porous flow and the transition between them. (a–b) Snapshots of the pressure distribution in the model box with fluid influx from below: (a) for three different fluid–pressure diffusion coefficients D with $D = 0$ (no diffusion), $D = 2 \times 10^{-6}$ (slow diffusion) and $D = 1 \times 10^{-4}$ (fast diffusion), and (b) for three time steps of the simulation with $D = 2 \times 10^{-6}$, where a hydrofracture reaches the top of the model at time $t = 1$. With time the pressure diffuses into the drained parts of the model and the initially sharp boundary becomes fuzzy. (c) Mean pressure in the model box versus time. A small diffusion coefficient produces irregular and intermittent behaviour. A high diffusion coefficient produces periodical pressure fluctuations. Modified after figures 3 and 4 of de Riese *et al.* (2020).

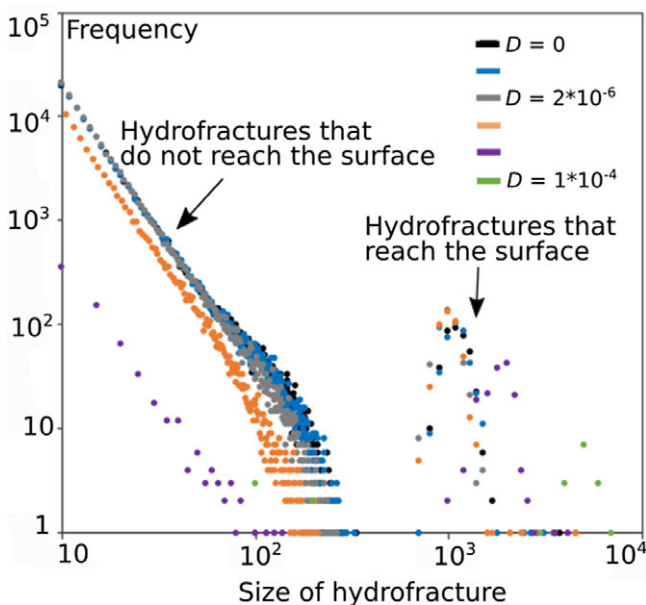


Fig. 10. Frequency distributions of hydrofracture sizes (area) for different pressure diffusion coefficients (D). Hydrofractures that do not reach the surface of the model follow a power law distribution as they plot on a straight line in the log–log plot. Modified after de Riese *et al.* (2020).

development of a tipping point or a bifurcation (Sornette, 2009). They are linked to the small hydrofractures that self-organize the fluid–pressure distribution, trigger avalanches and therefore initiate large fluid–escape events (Bons *et al.* 2009; de Riese *et al.* 2020). These large fluid–escape events transport very large fluid volumes with a high velocity from depth to shallow levels in the crust, where they can form hydraulic breccias. If the ascent of fluid is fast enough, as in the case of hydrofracture propagation (Bons, 2001), fluids would not be able to decrease their temperature significantly and, as they may have high concentrations of dissolved elements, these fluids could deposit ores and cause extensive rock alteration. The Black Forest ore province (SW Germany) is characterized by a large number of small ore deposits (Staudé *et al.*

2009), which could have been produced by a large number of small fluid escape events (Bons *et al.* 2014). It is of interest to note that the volumes of these deposits follow a power law (fig. 4 in Staudé *et al.* 2009).

4. When is a fracture or vein a hydrofracture?

In this section we address the question how to determine whether a fracture or vein found in the geological record was formed as a hydrofracture, and thus could be an indicator of elevated fluid pressure at the time of its formation. Hydrofracturing may appear obvious in the case of igneous dykes, i.e. originally magma-filled fractures. With the frozen magma still preserved inside the fractures it is clear that the fluid ‘magma’ caused or at least played a significant role in the formation, opening and propagation of the fractures. In other cases, the question may be more difficult to answer.

4.a. Hydrofractures and depth

Extensional veins are often assumed to have formed from tensional failure (see discussion below), and therefore to indicate elevated fluid pressure or hydrofracturing (e.g. Cobbold & Rodrigues, 2007) on Earth, but also on Mars (e.g. Caswell & Milliken, 2017; Kronyak *et al.* 2019). The rationale is that the Mohr circle for stress must touch the failure envelope in the negative normal stress region to induce extensional (pure mode I or hybrid) fractures. This implies that both the mean stress (midpoint of the Mohr circle) and the differential stress (the diameter of the Mohr circle) are limited in magnitude, because a larger Mohr circle would touch the failure envelope in the non-dilatant shear–fracture regime. Without an elevated fluid pressure, a small mean stress is only found at shallow depths. At greater depths this can only be achieved with an elevated fluid pressure. Etheridge (1983) used this logic to argue that under metamorphic conditions fluids are usually overpressured and differential stresses are limited because extensional veins are common in metamorphic rocks.

Extensional fractures that formed under metamorphic conditions, at depths greater than *c.* 10 km, are hydrofractures as they can only occur when the fluid pressure is raised significantly.

However, for extensional fractures formed at shallow depths it is less clear whether they are hydrofractures as they could potentially also be caused by tectonic stresses without a reduction of the effective stresses due to an elevated fluid pressure. We define the critical depth (z_{crit}) as the depth below which extensional fractures can be assumed to be hydrofractures. Both Sibson (2000a) and Gudmundsson (2011) use $g \rho_{rock} z_{crit} = -3T$ that is derived from the Griffith criterion to obtain a maximum depth of 1–2 km for purely tectonic extensional fractures, i.e. those that formed without a contribution of the fluid pressure. Both authors base their outcome on the generally low tensional strengths of bulk rocks, between –3 and –6 MPa according to Gudmundsson (2011). However, Hooker *et al.* (2015) describe quartz veins that they argue formed as infill of c . 6 km deep tectonic fractures in the absence of an elevated fluid pressure. The authors used $c = 60$ MPa, $T = -25$ MPa and $\mu = 0.6$.

Above we defined hydrofractures as those fractures whose failure was caused primarily by fluid overpressure (P_f). We now define ‘primarily’ as $P_f \geq (\sigma_1 - \sigma_3)/2$, with σ_1 and σ_3 the effective stresses at the point of failure to take into account that the Mohr circle can change in size as fluid pressure changes (Fig. 2). This means that for a hydrofracture the shift of the Mohr circle is larger than the radius of the Mohr circle at the moment of failure.

The Griffith criterion only takes T into account and not the angle of internal friction for $\sigma_n > 0$. Here we propose to also use the criteria for shear failure (c and μ or ψ), in addition to T . We neglect hybrid failure, but the poorly constrained hybrid failure criteria allow this simplification. The intention is to find a rough depth below which extensional fractures are most likely hydrofractures. Using these failure criteria, one can find the Mohr circle that touches the failure envelope both at the tensional failure criterion and at that for shear failure (orange circle in Figs 1c and 11a) (Behrmann, 1991). A smaller circle positioned further left will only cause tensional failure, while a larger circle further to the right will only cause shear failure. The principal stresses for a circle that touches the shear failure criterion are given by:

$$\frac{(\sigma_1 - \sigma_3)}{2} \cos \psi = c + \tan \psi \left(\frac{\sigma_1 + \sigma_3}{2} - \frac{\sigma_1 - \sigma_3}{2} \sin \psi \right) \quad (18)$$

The circle reaches the tensional failure criterion at the same time, giving $\sigma_3 = T$, giving:

$$\sigma_1 = \frac{\frac{2c}{\tan \psi} + \left(\frac{\cos \psi}{\tan \psi} + 1 + \sin \psi \right) T}{\frac{\cos \psi}{\tan \psi} - 1 + \sin \psi} \quad (19)$$

In an Andersonian stress configuration the vertical stress at depth z is $\rho_{rock}gz$, but the horizontal stress can deviate from this value. A vertical extensional fracture can form if the horizontal effective stress is reduced enough to reach T . We combine the criteria that at the critical depth both tensional and shear failure occur (Eq. 19) and that the fluid pressure is half the diameter of the Mohr circle to obtain:

$$\sigma_1 + P_f = \sigma_1 + \frac{\sigma_1 - T}{2} = \rho g z_{crit} \Leftrightarrow z_{crit} = \frac{3\sigma_1 - T}{2\rho g} \quad (20)$$

Note that we only deal with stress conditions and can thus use Terzaghi’s principle without taking into account poroelastic effects. For these the reader is referred to Olson *et al.* (2009).

Combining Eqs (19) and (20) now gives the critical depth, below which fluid pressure must have contributed at least 50 % to tensional failure, as a function of c , T and ψ . We see in Figure 11 that z_{crit} strongly depends on the assumed failure criteria and can theoretically reach well over 5 km, especially if cohesion is high. However, if the effective tensional strength and cohesion of bulk rocks are indeed rather small, much shallower critical depths are obtained, such as the ~1 km of Gudmundsson (2011) or ~2 km of Sibson (2000a). As our derivation of z_{crit} is not for a dry rock, but for a 50 % contribution to failure of fluid pressure, we suggest using a critical depth range of c . 2–3 km below which extensional fractures under most circumstances must have formed with a significantly elevated fluid pressure and can thus be regarded as hydrofractures. This maximum depth of tensional failure without high fluid pressure roughly coincides with the calculations of Bourne (2003) for the formation of extensional fractures in multi-layer systems that are subjected to remote compression in which alternating beds have contrasting elastic properties. This of course cannot simply be applied to extensional fractures that form part of a fracture network, like extensional jogs in a shear fracture. The above Mohr–Coulomb construction of an isotropic rock does not apply to such more complex systems (Koehn *et al.* 2005). Based on similar approaches to those presented in this section, other studies proposed shallow depths for the formation of hydrofractures for vein networks, using the elastic crack theory and the vein mean aspect ratio (Phillip, 2012).

Mineral veins in sediments on Mars have been interpreted as hydrofractures (Kronyak *et al.* 2019). However, gravitational acceleration on Mars is only 3.721 m s^{-2} . Although the olivine-rich clastic sediments may have a higher density, the product of rock density by g on Mars is less than half that on Earth, when using rock densities of 3000 kg m^{-3} and 2500 kg m^{-3} , respectively. This means (Eq. 20) that z_{crit} on Mars is more than double that on Earth for the same failure criteria. Unless the depth of formation of the Mars veins can be constrained, care must be taken in using the presence of veins as evidence for hydrofracturing.

The above certainly does not imply that all fractures that formed at a shallower depth than z_{crit} are not hydrofractures. It only means that the mere presence of extensional fractures is not enough to state that fluid pressure was the dominant cause for the fracturing. Additional information can of course further constrain the fluid pressure state. In a basin at rest, for example, one knows that tectonic stresses cannot have caused the fracturing, as otherwise it would not be at rest. Horizontal extensional fractures in such a basin must have formed from fluid overpressure (Eq. 10). However, on Mars, for example, palaeostress conditions are poorly constrained and meteorite impacts may also have contributed significantly to fracturing.

4.b. Veins as potential fossil hydrofractures

Formerly open fractures in the geological record are typically identified as veins that are originally open fractures in which the fluid-filled space is now filled by minerals that precipitated from a fluid (Bons *et al.* 2012). There is no reason to assume that open fractures are always filled with minerals. Instead, they can also remain open, or completely or partially close again. Becker *et al.* (2010), for example, show that quartz veins in the East Texas Basin (USA) remained (partially) open for 48 Ma. The opposite would be the case in mobile hydrofractures (Bons, 2001), where the fracture propagates and opens at its upper end while closing at its lower one. This process is assumed to be rapid enough to not allow

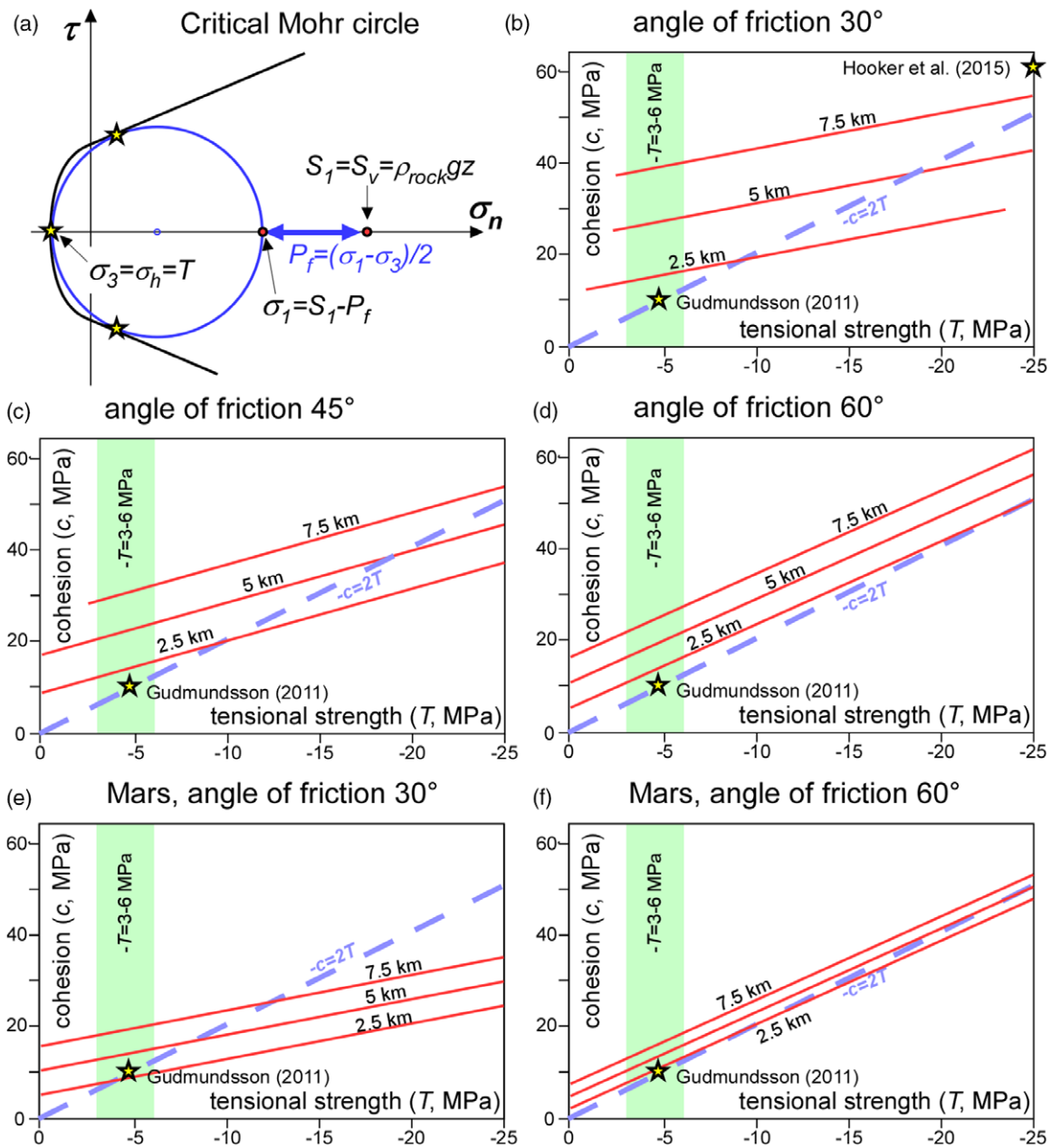


Fig. 11. Maximum depth of tectonic extensional fractures. (a) Mohr-Coulomb diagram with Mohr circle that touches (stars) the failure envelope at both the criterion for tensile failure and for shear failure. When P_f is more than the radius of the Mohr circle, we regard failure as dominantly caused by the elevated fluid pressure, i.e. a hydrofracture. The depth at which this occurs is z_{crit} . (b-d) Graphs of different values of z_{crit} as a function of cohesion (c) and absolute tensile strength (T), and for different angles of internal friction for the Earth's gravitational acceleration of $g = 9.81 \text{ m s}^{-2}$ and an assumed rock density of $\rho_{rock} = 2500 \text{ kg m}^{-3}$. (e-f) Same graphs for Mars with $g = 3.721 \text{ m s}^{-2}$ and $\rho_{rock} = 3000 \text{ kg m}^{-3}$.

for any significant mineral precipitation to occur in the time that at any one location the fracture is open. Especially for quartz these assumptions seem warranted considering the slow growth rates of $<1 \text{ mm Ma}^{-1}$ up to 250°C reported by Lander and Laubach (2015). These authors, but also for example Laubach *et al.* (2004), describe how cracks can be partially filled with bridging crystals that leave fracture porosity in between, as revealed by cathodoluminescence. In some cases it may be possible to recognize a formerly open fracture that subsequently closed again, maybe only partially filled with minerals, by the distortion of the rock around the former fracture (Fisher & Brantley, 1992; Bons *et al.* 2008) (Fig. 12).

Veins can provide indications of the stress and fluid pressure conditions at the time of their formation, firstly, by their shape or orientation, and secondly by their internal structure. Moreover, fluid inclusions within vein cement can be used to systematically unravel palaeo-fluid pressures (Becker *et al.* 2010). Durney and Ramsay (1973) introduced the basic terminology and classification of internal vein structures that is still widely used today. It consists of (i) the growth direction of vein crystals relative to the wall rock, and (ii) the morphology of these crystals. This results in three main vein categories (Bons *et al.* 2012): first, syntaxial veins with blocky or elongate blocky crystals that consistently grow from the wall-rock substrate towards the middle of the vein

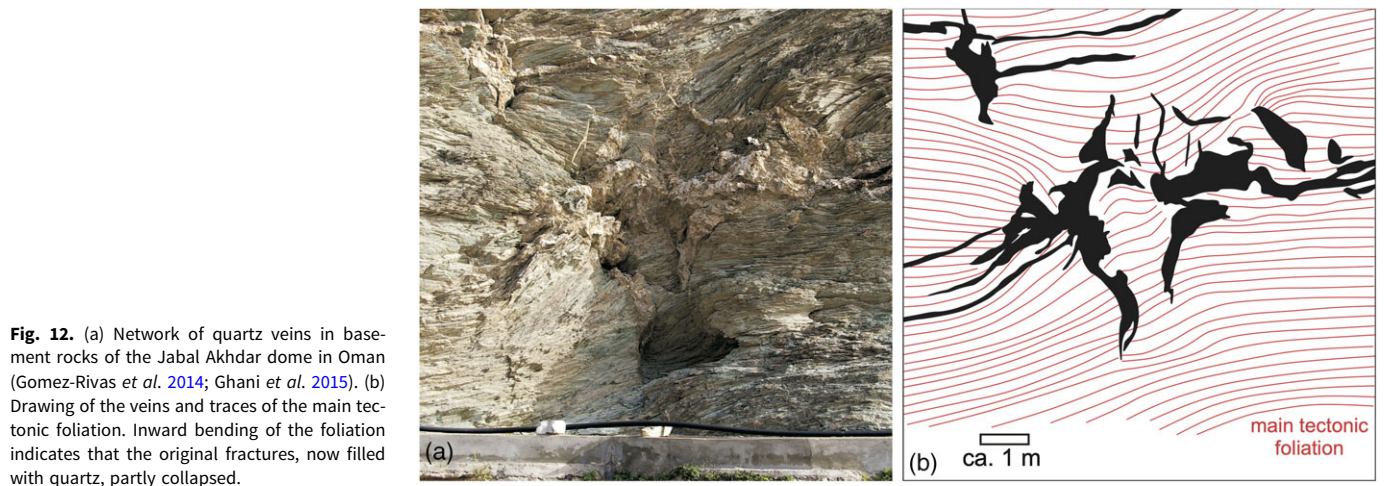


Fig. 12. (a) Network of quartz veins in base-metamorphic rocks of the Jabal Akhdar dome in Oman (Gomez-Rivas *et al.* 2014; Ghani *et al.* 2015). (b) Drawing of the veins and traces of the main tectonic foliation. Inward bending of the foliation indicates that the original fractures, now filled with quartz, partly collapsed.

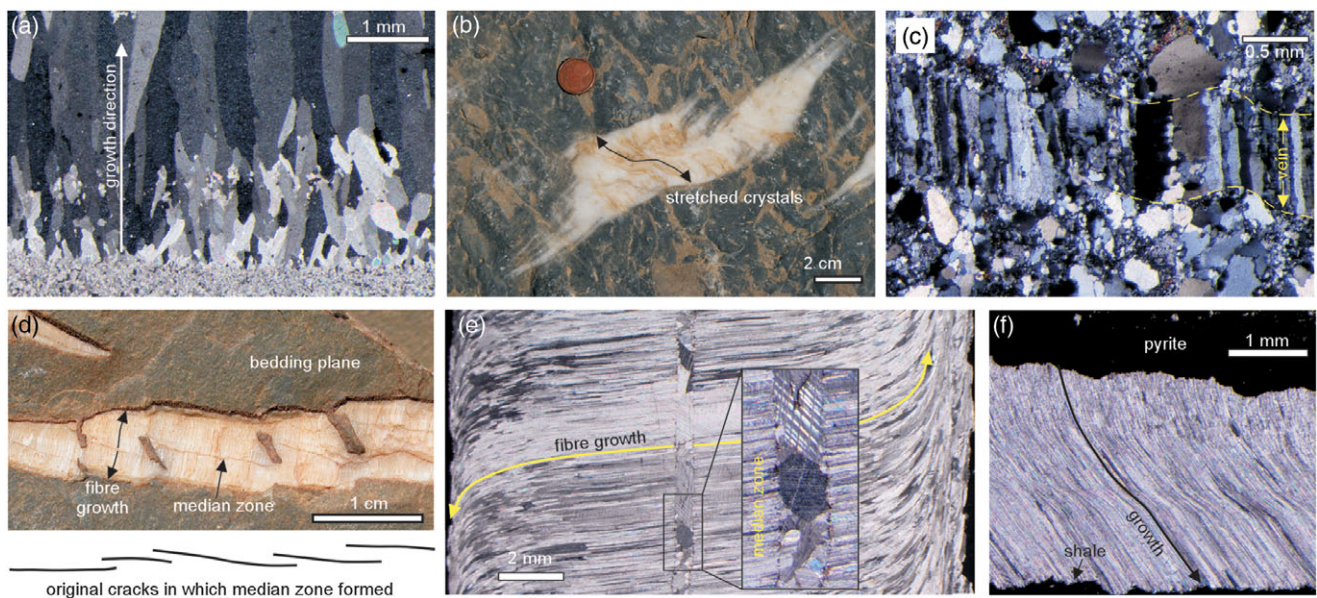


Fig. 13. Representative images of (a) syntaxial, (b–c) stretching, and (d–f) antitaxial or beef vein types. (a) Syntaxial calcite vein from Biure (NE Spain) showing clear growth competition in the upward growth direction. (b) Stretching vein from the Jabal Akhdar dome, Oman, with long stretched calcite and quartz crystals. The tips of the vein show that the vein formed by many individual crack–seal events. (c) Quartz vein with stretched crystals with parallel serrate boundaries, indicating multiple crack seal events. Yudanmutana, Mount Painter Inlier, South Australia. (d) Antitaxial, fibrous (beef) vein from Oppaminda Creek, Mount Painter Inlier, South Australia. The vein formed by outward growth from originally narrow en échelon crack–fills shown below. (e) Antitaxial fibrous vein from same locality, showing symmetry of curvature of the smooth fibres (compare with (c)) on both sides of the median zone, which itself has a very different internal structure. (f) Fibrous vein where the fibres are not seeded on a median zone, but on a layer of pyrite. Minor coarsening of the smooth fibres shows the growth direction, with the fibre tips growing against the host-rock shale. Drill core sample of the Lower Silurian Longmaxi Formation shale, Luzhou Block, Southern Sichuan Basin, China.

(Fig. 13a); second, stretching, or ataxial veins with stretched crystals that grew by repeated fracturing and sealing (Ramsay, 1980) and that may not show any preferred growth direction (Fig. 13b–c); finally, antitaxial veins with fibrous crystals that grow against the wall rock as the vein widens (Fig. 13d–e).

The crack–seal theory of Ramsay (1980) is fundamental to understanding the formation of veins from fractures. He showed that veins can form by repeated failure that results in opening of a fracture (the ‘crack’ stage), and subsequent filling of the fluid-filled space with minerals (the ‘seal’ stage). Mineral precipitation is usually by epitaxial overgrowth of mineral grains at the fracture surfaces, as can be seen from the optical continuity between old and new growth stages (Urai *et al.* 1991; Laubach *et al.* 2004; Späth *et al.* 2021). A crack–sealing cycle can occur once for a vein, but also

many times, each time adding a slice of mineral precipitate to the widening vein. If the width of the open fracture is large relative to the width of the seed crystals for the mineral veins, we usually observe competitive growth of vein crystals from the fracture surfaces into the fracture space. As a result, some crystals outgrow their neighbours, and the mean crystal width increases towards the middle of the vein (Fig. 13a). This is the classical syntaxial vein geometry in which the crystals typically have blade-like or elongate-blocky shapes (Durney & Ramsay, 1973; Fisher & Brantley, 1992; Hilgers *et al.* 2001; Okamoto & Sekine, 2011; Späth *et al.* 2021). Although the original work of Ramsay (1980) and many other subsequent papers assume that the whole crack fills with minerals before the next crack event, this is not always the case, especially under diagenetic conditions. Isolated crystals may

already span the crack, while leaving open pore space in between (Laubach *et al.* 2004; Kling *et al.* 2017; Späth *et al.* 2022), or cracks may only fill completely near their tips, but not in their wider central parts (Bons *et al.* 2012).

The crack–seal cycle can also occur many times during the growth of a single vein. The narrow width of the open fracture in each individual crack–seal event inhibits growth competition (Hilgers *et al.* 2001). Furthermore, the location of each new open fracture may differ from that of the previous one. As a result, individual vein crystals are stretched by inserting slice after slice of epitaxially grown mineral in the gap formed in the crystal each crack–seal cycle. These vein crystals therefore do not usually show a consistent widening in one direction, but can become long and narrow (Fig. 13b), often called ‘fibres’, although we prefer the term ‘stretched crystals’ (Bons *et al.* 2012). The veins are termed ‘stretching veins’ or ‘ataxial veins’ (Passchier & Trouw, 2005), as their crystals show no consistent growth direction. Repeated crack–sealing can be recognized by the stretched-crystal morphology, where the boundaries between individual crystals are often serrate on the length scale of the individual fracture widths (‘radiator structure’; Fig. 13c), and the presence of fracture-parallel bands of fluid inclusions, wall-rock particles or secondary minerals (Ramsay, 1980; Renard *et al.* 2005). It should also be noted that an open crack need not fill evenly, but some individual crystals may outgrow others to form bridges across the crack and incrementally restore cohesion until a new failure event occurs (Laubach *et al.* 2019; Späth *et al.* 2022). Crystal morphology in crack–seal veins can therefore be variable and repeated crack–sealing may sometimes only be revealed with cathodoluminescence (Laubach *et al.* 2004; Gale *et al.* 2010). Syntaxial and ataxial vein growth are end members of a continuum, and both growth modes may operate in a single vein (Bons *et al.* 2012).

Recognizing crack–sealing in veins is important as each crack–seal cycle represents a point in time where the stress and fluid-pressure conditions were such that a dilatant fracture could form to provide the space for subsequent sealing by mineral growth. It is therefore also of equal importance to recognize those veins whose internal structure does not indicate crack–sealing.

Some veins consist of distinctly fibrous crystals that are aligned parallel to each other and that have smooth boundaries. They are often referred to as ‘beef veins’, as the fibrous texture is reminiscent of beef (Buckland & De La Beche, 1835). Gypsum, calcite and quartz are the most common minerals to form beef veins (Cobbold *et al.* 2013). Durney and Ramsay (1973) introduced the term ‘antitaxial’ for veins in which the vein-filling crystals grow outwards towards the vein/wall-rock interfaces (Fig. 13d). Crystal growth in antitaxial veins is seeded on what they termed a ‘median line’, but which Oliver and Bons (2001) termed a ‘median zone’, as it usually has a finite width (Fig. 13e). Antitaxial veins can be also called beef veins, as their vein crystals are smooth and fibrous. In the literature, the term ‘beef’ is often used for bedding-parallel fibrous veins, while ‘antitaxial’ is more often used for fibrous veins in general orientations. Beef veins may lack a median zone, which forms part of the definition of antitaxial veins (Durney & Ramsay, 1973; Passchier & Trouw, 2005; Bons *et al.* 2012). It should also be noted that the term ‘fibrous’ is sometimes used for any elongate vein crystals (e.g. Cox, 1987; Zhang *et al.* 2015) and then erroneously compared to antitaxial or beef veins, because these are fibrous. The term ‘fibrous’ should therefore only apply to very to extremely elongate crystals with parallel smooth boundaries (Oliver & Bons, 2001).

Many authors recognized the association of fibrous calcite (\pm quartz) veins with hydrocarbon generation during thermal maturation of organic matter (Bredehoeft *et al.* 1976; Osborne & Swarbrick, 1997; Cobbold & Rodrigues, 2007; Cobbold *et al.* 2013; Zanella *et al.*, 2015a; Wang *et al.* 2018; Hooker *et al.* 2020). Fibrous calcite veins are most common in organic carbon-rich shales (Fig. 13f) and often contain solid bitumen inclusions or hydrocarbon inclusions, which are further indications that the vein formation was synchronous with hydrocarbon generation (Zanella *et al.* 2015b; Wang *et al.* 2018; Su *et al.* 2021). The assumption that fibrous veins are formed by extensional fracturing has led the aforementioned authors and others (e.g. Cosgrove, 2001) to infer that these veins indicate hydrofracturing due to fluid overpressure, possibly caused by hydrocarbon generation during thermal maturation of organic matter. If the veins are parallel to horizontal bedding, this would imply that the fluid pressure must have exceeded the vertical overburden load (Section 3.a.2). However, as discussed by Cobbold *et al.* (2013), it is far from certain that fibrous crystal growth is the result of crack–sealing.

It was already suggested by Taber (1918) that growth must have been continuous, with the crystal-growth front at all times keeping track with the diverging wall rock (Durney & Ramsay, 1973; Urai *et al.* 1991). This is consistent with the smooth fibre boundaries and lack of suppression of growth competition (Mügge, 1928; Hilgers *et al.* 2001; Bons & Montenari, 2005). A further argument against growth of the fibres in an open fracture is that fibrous veins can grow simultaneously on both sides of a vein and it seems mechanically improbable that two parallel fractures exist on both sides of a growing vein (Bons & Montenari, 2005). The simultaneous growth on the outer surfaces of antitaxial veins is particularly conspicuous at intersections of antitaxial veins of different orientations. Here we can observe that both the old and new generation keep widening at their outer surface (fig. 7 in Oliver & Bons, 2001).

This aggregate of arguments suggests that fibrous growth occurs in the absence of open fractures (Taber, 1918; Mügge, 1928; Bons & Jessell, 1997; Means & Li, 2001; Oliver & Bons, 2001; Wiltschko & Morse, 2001; Luan *et al.* 2019; Meng *et al.* 2019; Su *et al.* 2021). It should be noted that median zones tend to have a different microstructure, typically one that does indicate crack–sealing (Fig. 13e), which led Bons & Montenari (2005) to propose that fibrous veins can be seeded on (narrow) crack–seal veins, but that fibrous growth subsequently undergoes a switch in the growth mechanism without crack–sealing (Su *et al.* 2021). However, some fibrous veins lack a median zone (Fig. 13f) and they may thus never have experienced any crack–sealing. Instead, the fibrous crystals appear to be seeded on a bed interface or lamination. A number of driving forces for fibrous growth in the absence of an open fracture have been suggested, such as the force of crystallization (Means & Li, 2001), concentration gradients due to stress or pressure gradients that drive dissolution–precipitation reactions (Fletcher & Merino, 2001; Bons & Montenari, 2005), or even microbial activity (Bons *et al.* 2007).

As the mechanism of fibrous or beef growth remains enigmatic, care should be taken before inferring fluid pressure from such veins and they should not be automatically equated with hydrofractures. We favour distinguishing between the conditions of (i) vein initiation where the median zone (even when completely on one side) is formed from (ii) the subsequent fibrous growth by which the vein widens. Geometry, orientation and internal microstructure of the median zone may indicate a significantly elevated fluid pressure at

time of formation. In particular, the median zones of horizontal fibrous or beef veins in organic-matter-rich shales are probably the result of elevated fluid pressure (Eq. 10; Fig. 2b) due to hydrocarbon release (see references above). However, the ‘Taber school’ (based on Taber, 1918) argues that the outer vein surface is not a crack, but a cohesive interface, where the fibres grow against the wall rock. Whether they do will depend on the ambient tectonic stress (Fletcher & Merino, 2001) and probably fluid pressure as well, and of course the rock type, minerals involved, etc. Still if the fibres grow in the absence of a fracture, the resulting fibrous vein cannot be called a hydrofracture.

4.c. Breccias

Breccias are rock masses composed of broken rock fragments. Breccias can be of a variety of origins. Aside from impact and sedimentary breccias, or those formed by tectonic diminution in faults due to tectonic stresses (e.g. Sibson, 1986; Keulen *et al.* 2007; Mort & Woodcock, 2008), they can also develop by intensive hydrofracturing due to fluid overpressure as of interest here (Laznicka, 1989; Jébrak, 1997; Lorilleux *et al.* 2002; Weisheit *et al.* 2013a). Long-distance transport of clasts, and structures that indicate fluidization, suggest that fluid flow velocities may be as high as m s^{-1} (Oliver *et al.* 2006b). Eichhubl (2000) and Okamoto & Tsuchiya (2009) estimated fluid velocities of 0–0.1 m s^{-1} , while Oliver *et al.* (2006b) estimated velocities of 5 m s^{-1} in the case of a fluidized breccia with m-sized clasts.

To give an example, the Hidden Valley breccia in the Northern Flinders Ranges of South Australia is a massive hydrothermal breccia with a size of *c.* 10 km^2 in outcrop (Weisheit *et al.* 2013a). The breccia features a continuous power-law distribution of clast sizes that span over six orders of magnitude. Mixed clasts that were originally several km vertically apart are observed. Using thermogeochronology, Weisheit *et al.* (2013b) inferred that the breccia formation extended over a period of >150 Ma during the exhumation of basement gneisses by >12 km. The estimated total fluid budget responsible for the development of this breccia is *c.* 20 km^3 (Weisheit *et al.* 2013a). Biotite dehydration seems to be the main fluid source in this case.

To distinguish hydraulic breccias from other types of breccias, the clast size morphology and distribution can be used, in particular their fractal dimension, which is related to the rock fragmentation process (Blenkinsop, 1991; Jébrak, 1997; Lorilleux *et al.* 2002; Barnett, 2004; Keulen *et al.* 2007; Weisheit *et al.* 2013a). The fractal dimension for the size distribution is defined as the absolute power-law exponent (*m*) that is obtained when the number of breccia clasts that are larger than a certain size is plotted against that size (see e.g. Blenkinsop (1991) for the calculation). Weisheit *et al.* (2013a) found a constant exponent m_{2D} of about 1 (using the two-dimensional clast area as the measure of size) for clast areas from *c.* 1 mm^2 to almost 1 km^2 . The power-law distribution evidences that the fragmentation process is scale-invariant (Turcotte, 1986), and also emphasizes the dynamical behaviour of the fluid flow that produced the breccia. Jébrak (1997) and Barnett (2004) found that hydraulic brecciation results in a small exponent ($m \approx 1$), whereas wear abrasion and shear results in larger exponents ($m \approx 2-3$), meaning there are relatively many small clasts compared to large ones. The small exponent of about 1 obtained for the Hidden Valley breccia by Weisheit *et al.* (2013a) thus indicates it formed by hydraulic brecciation. Round clast shapes and the absence of tectonic structures further confirm a hydraulic origin (Weisheit

et al. 2013a). Another indicator is the strong alteration of this breccia which indicates the passage of large fluid volumes.

Weisheit *et al.* (2013a) argued that, assuming a porosity of 10% and a flow rate of 1 m s^{-1} , the estimated cumulative duration of flow through each part of the breccia would be *c.* 2×10^4 s, which is less than a day. Even if the flow rate were much smaller, the total flow duration would still be a minute fraction of the tens of million of years it took to form the breccia. The required fast fluid flow must therefore be highly intermittent, with short bursts of flow and very long periods of fluid pressure build-up. The Hidden Valley brecciation could be equivalent to the extremely large fluid escape events in the numerical simulations of de Riese *et al.* (2020) and shown in Figures 9 and 10 with a high proportion of fluid pressure diffusion to accumulate the large fluid volume to create the 10 km^2 breccia.

4.d Recognizing hydrofractures in the geological record

This subsection provides some examples of hydrofracturing in different tectonic settings. Examples of different vein sets from the Ligurian Units near Sestri Levante, Italy, are given in Figure 14. The units represent the marine Palombini shales that are thrust first southwards and later eastwards towards the Apennine mountain chain. Veins in the units show a variety of geometries that point towards different importance of fluid overpressure during the initial fracturing, assuming the veins represent at least partly the original fracture pattern. Examples for high fluid overpressure and thus real hydrofractures include very intense veining in soft layers and within small sheared units (Fig. 14a–b), geometries where bedding-parallel and -perpendicular veins switch even though the veins are of the same age (Fig. 14a), and early bedding-parallel veins (Fig. 14d). Examples where differential stresses dominated the pattern include conjugate vein sets on bedding surfaces (Fig. 14c), fracture boudinage type veins that fractured layers (Fig. 14d), and extensional fold-axis-parallel veins that may have developed during folding (Fig. 14c). All the latter examples may have needed local or larger-scale fluid overpressure to overcome tensile or shear stresses, but fluid overpressure does not seem to have dominated the pattern. Therefore, we would not term them ‘hydrofractures’. Real hydrofractures that develop due to a dominance of fluid overpressure are shown in the simulations in Figure 4. Figure 4a–b show the development of horizontal fractures in layers or in a sedimentary basin when the fluid overpressure increases at the same rate in all nodes. This pattern represents the developing bedding-parallel veins in Figure 14d, which were produced by fluid overpressure. The more complicated branching pattern with horizontal and vertical fractures as well as potentially many small and very closely aligned fractures develops in the simulations when a local region in the rock is overpressured (Fig. 4c). If the pressurizing fluid is locally produced in layers within laterally confined cells, then a combination of the patterns shown in Figure 4c and e may develop, which also fits the pattern in Figure 14a. The pattern shown in Figure 14b that develops in a small fault zone is extreme and potentially would be a further development of the simulation shown in Figure 4c in combination with shearing. It could also be compared with the numerical hydraulic breccia pattern shown in Figure 5.

Another well-studied area with examples of the effect of fluid pressure on fracture and vein formation is the Jabal Akhdar Dome in the Oman Mountains (Oman) (Fig. 15). The complex tectonic evolution of this area can be traced from the cross-cutting relationships of different faults and sets of calcite veins

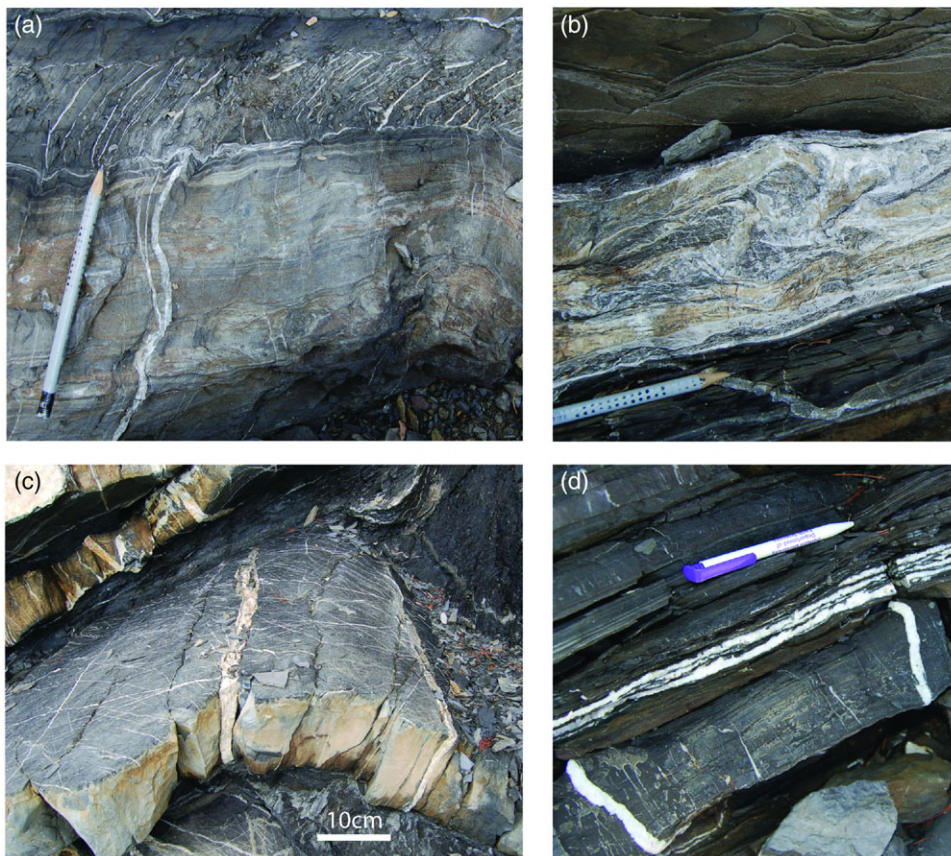


Fig. 14. Veins from the Ligurian Units at Sestri Levante, Italy, representing different effects of the fluid pressure assuming they represent the initial fracture geometries. (a) Complex inter-fingering between bedding-perpendicular and bedding-parallel veins. (b) Intense veining in a small thrust fault zone. (c) Veins in folded layers with early conjugate and later fold-axis-parallel veins. (d) Early bedding-parallel veins and fracture boudinage type veins in a layer.

(Gomez-Rivas *et al.* 2014). The area was first buried >8 km under the Semail ophiolite and Hawasina nappes. It subsequently underwent strike-slip deformation from the Late Cretaceous to the Eocene due to the northwards movement of the neighbouring Indian plate. Although exhumation by erosion may have started during this time, the main exhumation happened after the main veining events discussed below. Strike-slip deformation led to the formation of intense calcite vein networks in conjugate sets. Such veins are hosted in limestones of the Cretaceous Shams, Nahr Umr and Natih Fm., just below the Muti Fm., which likely acted as a regional seal for interstitial fluids and fluids derived from the basement (Fig. 12). Extensional and hybrid veins that formed at depths around 8 km would require a significant fluid overpressure and may be assumed to have formed as hydrofractures (Section 4a). A hydrofracture origin is consistent with zones of intensive fracturing that resulted in the formation of veins with chaotic orientations (Fig. 15a–c). In this area there are also pavements (Fig. 14d–e) that contain networks of calcite veins typically arranged in an échelon conjugate sets (and with crack–seal microstructures; Fig. 13b) (Bons *et al.* 2012; Gomez-Rivas *et al.* 2014) that formed under a rotating strike-slip stress field. Individual vein segments are oriented at a very low angle with respect to the principal compressive stress, while the acute angle between conjugate sets is also low (typically 15 – 30°). These orientations reveal that such vein systems formed as hybrid fractures, with some individual segments also formed as extensional fractures, again indicating a system characterized by high fluid pressure. However, with these more regular vein sets that indicate a tectonic contribution to fracture orientations, it becomes difficult to ascertain the actual role of

fluid overpressure, especially where the depth of fracturing is not well constrained.

Palaeostress inversion techniques aim to unravel the stress fields under which fractures, faults and other geological structures (e.g. veins, stylolites) formed. Some studies consider fluid pressure as a key parameter for palaeostress determination. Jolly and Sanderson (1997) propose and demonstrate a Mohr circle construction for the analysis of veins or dykes that allows to graphically estimate stress magnitudes and the relative fluid pressure, providing the range of fracture orientations that can open, together with their opening directions. This method is based on the approach by Delaney *et al.* (1986) that assumes that fractures are opened by fluid pressure when it exceeds the normal stress on the fracture planes. Yamaji *et al.* (2010) apply the same principle to propose a method for the estimation of the stress of state from clusters of veins formed from multiple events of ascending warm fluids with variable fluid pressures, assuming that most batches arrive at a lower fluid pressure than the maximum one. For that, they evaluate the stress state of each vein cluster from an orientation distribution that best fits the vein orientation. Other authors carried out palaeostress determinations from veins, and palaeofluid pressure determinations from fluid inclusion microthermometry data (André *et al.* 2001) or in combination with geothermometers (Jaques & Pascal, 2017). The latter authors applied this method to a case study from the Panasqueira Mine (Portugal), to conclude that horizontal mode I veins formed as hydrofractures at a lithostatic fluid pressure at depths of *c.* 10 km in a compressive stress regime. The reader is referred to Pascal (2021) for a thoughtful review of palaeostress inversion techniques.

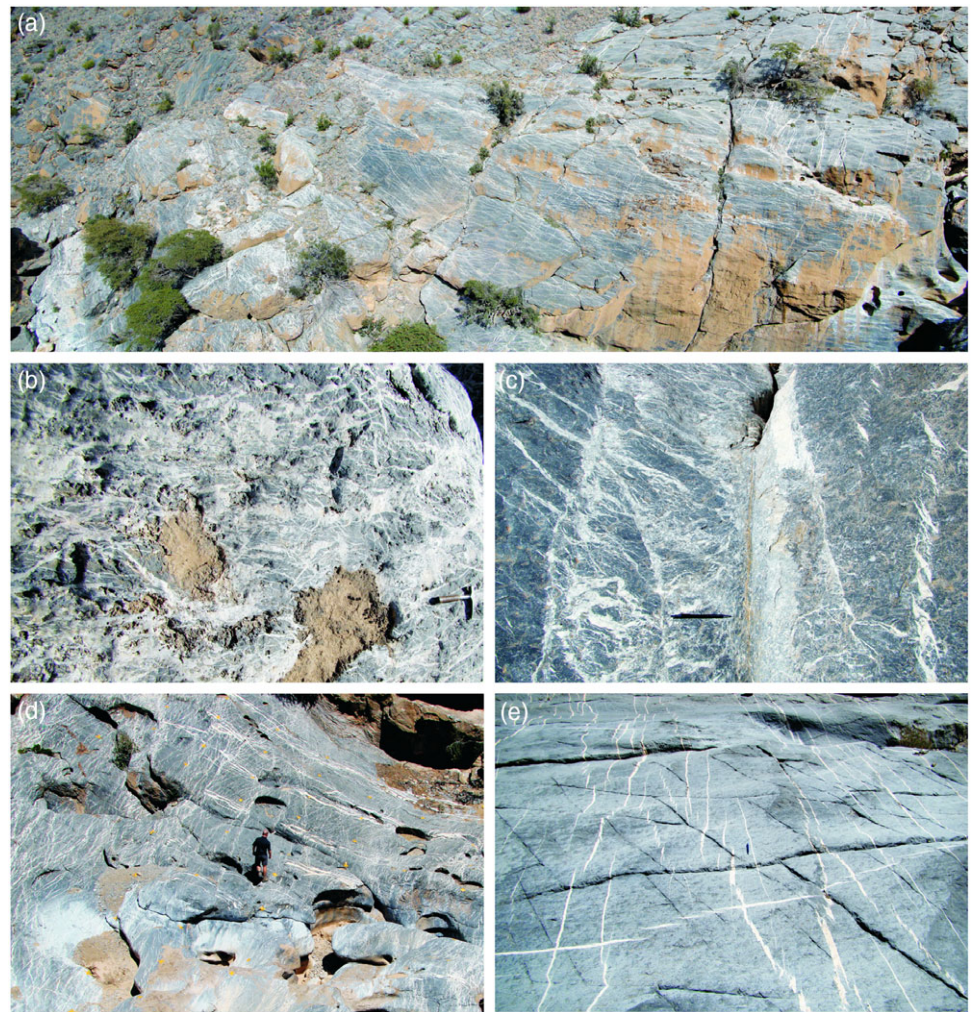


Fig. 15. Examples of calcite veins hosted in limestones of the Natih Formation from the Jabal Akhdar dome (Oman Mountains, Oman), which are interpreted to have formed in a system with relatively high fluid pressure. (a) Dense calcite vein networks with some veins showing systematic orientations while others form a chaotic mesh (Gorge pavement). (b) Detail of a zone with intense and chaotic calcite veining in (a). (c) Damage zone of an outcrop-scale strike-slip fault showing a dense mesh of calcite veins with variable orientations (Wadi Dam). (d) Pavement with different sets of systematically oriented conjugate crack-seal veins formed under different strike-slip stress fields (Wadi Guhl). (e) Detail of conjugate sets of en échelon strike-slip veins (Gorge pavement). The acute angle between both sets is typically in the range 15–30°, while individual segments form a very low angle with respect to the principal compressive stress. The dense vein meshes of (a), (b) and (c) clearly formed in a setting dominated by high fluid pressure at a certain depth, and thus formed by hydrofracturing. Systematically oriented strike-slip vein sets can be considered as formed from hybrid fractures in a system with relatively high fluid pressure, owing to their orientation with respect to σ_1 . For a detailed description of these veins see Gomez-Rivas *et al.* (2014).

5. Effects of hydrofractures in hydrocarbon and ore deposit systems and their relationship with geochemistry

Both natural and human-induced hydrofractures can either favour or constrain the origin, evolution and exploitation of hydrocarbons. Moreover, understanding the formation mechanisms of hydrofractures and being able to predict their zones of formation is also key for the exploration and production of ore deposits (e.g. vein stockworks and vein-type deposits; Liu, *et al.* 2017; Sun *et al.* 2021), to enhance the production of geothermal energy (e.g. Moska *et al.* 2021) and to ensure the safe geological storage of geo-energy products, such as captured CO₂, hydrogen, compressed air and natural gas (e.g. US Nuclear Regulatory Commission, 2009; Stork *et al.* 2015).

Human-induced hydrofracturing in hydrocarbon reservoirs has enabled two major innovations in the energy sector: (i) the enhanced recovery of reserves from producing fields, and (ii) the exploitation of unconventional reservoirs, i.e. those low-permeability, 'tight' reservoirs that cannot be exploited by using traditional extraction methods (including shale gas, tight sands gas and coal bed methane gas) (Bennion *et al.* 1996; Stanchits *et al.* 2011; Wang *et al.* 2014). Hydraulic fracturing is nowadays the principal technique for increasing and maintaining well productivity (Montgomery & Smith, 2010).

In the mining sector, hydrofracturing is also employed as a pre-conditioning and pre-weakening technique to induce caving and

fragmentation of the ore bodies in preparation for extraction (Katsaga *et al.* 2015; He *et al.* 2016). The occurrence of hydraulic fracturing is, however, also seen as a hazard during some types of mining operations. For example, during *in situ* leach uranium recovery, lixiviant excursions can take place through the formation and propagation of hydrofractures in the ore zone and surrounding rocks, giving rise to an unintended spread that may affect the groundwater quality near the well fields (US Nuclear Regulatory Commission, 2009). Natural hydrofracturing processes are also a key phenomenon for the formation and evolution of ore deposits. It is well known that ore deposits are often related to zones of localized deformation, such as fault zones, shear zones, fracture networks and other rock discontinuities (e.g. Groves *et al.* 2018; Chauvet, 2019). Hydrofracturing is an important mechanism for the generation of some such zones, and the resulting hydrofractures can act either as conduits or barriers to fluids that transfer heat and chemical components at different levels of the Earth's crust. In particular, those ore deposits genetically related to extensional fractures and that formed at a depth below 2–3 km from the Earth's surface are, according to what has been suggested above, the result of hydrofracturing processes. The role of hydrofractures as fluid baffles or conduits mainly depends on whether they are sealed by mineral precipitation or, alternatively, remain open. In the first scenario, fluid-pressure drops linked to failure events can trigger mineral precipitation, and if this process is repeated

over a geological time, it can give rise to multi-stage mineralizations of different types (e.g. Xiong *et al.* 2020; Sun *et al.* 2021). Otherwise, in the second scenario, the permeability enhancement produced by hydrofracturing can favour subsequent fluid circulation through fracture networks. However, not all fracture-related ore deposits are the result of hydrofracturing, and neither are all hydrofractures ore deposits. For example, Groves *et al.* (2018) suggested that the occurrence of hydrofractures in Neoproterozoic terranes could have caused high-pressure variations leading to gold deposition through related chemical responses and fluid un-mixing episodes. However, in the same tectonic settings, the existence of 'late fractures' (possibly hydrofractures) is also reported and linked to orogenic collapse, in all cases postdating the gold deposition (Vielreicher *et al.* 2016; Groves *et al.* 2018). Furthermore, when ore deposits are related to hydrofracturing, the cyclical evolution of fluid pressure and resulting failure events generally give rise to complex geochemical patterns that evolve from repeated depletion to enrichment patterns and from randomly distributed to spatially clustered structures, as demonstrated by Xiong *et al.* (2020) through numerical modelling. Recent advances in the understanding of the relationships between fluid composition, chemical reactions, fracture formation and fracture propagation demonstrate that, in the diagenetic regime (~50–200 °C), there are more profound interactions between these factors than assumed so far (see a review in Laubach *et al.* 2019).

6. Conclusions

Hydrofracturing, the process of rock failure that is primarily induced by an elevated fluid pressure, is an omnipresent tool in hydrocarbon and ore production, but also geothermal energy generation and underground storage of CO₂, natural gas or nuclear waste. Here we also show that most natural extensional fractures (pure mode I or hybrid) that formed below c. 2–3 km depth on Earth can, for typical rock mechanical properties, probably only have formed as hydrofractures.

We discuss the two main approaches to assess the effect on failure of an elevated fluid pressure: the effective stress according to Terzaghi's and Biot's theory. The two theories are not contradictory but apply depending on the stress and/or elastic strain boundary conditions.

Initial failure can be predicted with the Mohr–Coulomb–Griffith theory and appropriate effective stresses. Systems with fractures, however, evolve after fractures first form. Depending on the rate of overpressure generation, a system may reach an equilibrium in which fractures form and provide sufficient additional permeability to drain the fluid influx that caused the overpressure. Such systems can also become highly dynamic and self-organize. This leads to fluctuations in fluid pressure and fracture activity. We discuss how the interplay between porous flow and dynamic fracture flow can result in cyclical behaviour and major fluid drainage events.

Finally, we discuss, with examples, veins and breccias that are the products of hydrofracturing. Numerical models show that patterns of veins can be indications of hydrofracturing, especially chaotic or breccia-like vein patterns. However, we also emphasize that not all veins are former fractures, for example fibrous or 'beef' veins.

Supplementary material. To view supplementary material for this article, please visit <https://doi.org/10.1017/S0016756822001042>

Acknowledgements. This study was supported by research projects PID2020-118999GB-I00 and PGC2018-093903-B-C22 (Spanish Ministry of Science and Innovation (MCIN)/State Research Agency of Spain (AEI)). HT and DC acknowledge funding by the Chinese Scholarship Council (CSC) with grant numbers 202006440101 and 202006440128, respectively. EGE acknowledges the PhD grant 2021 FI_B 00165 funded by the Generalitat de Catalunya and the European Social Fund. EGE and EGR acknowledge funding provided by the Grup Consolidat de Recerca 'Geologia Sedimentària' (2017SGR-824). IN wishes to acknowledge funding provided by the DAAD: German Academic Exchange Service (DAAD), Section ST32, grant nr. 91731924. DK acknowledges funding by the Bavarian Ministry of Science and Art (StMWK) funded projects 'langfristig' and 'regional' of the Geothermal Alliance Bavaria (GAB). EGR acknowledges the Ramón y Cajal Fellowship RYC2018-026335-I, funded by the Spanish Ministry of Science and Innovation (MCIN)/State Research Agency of Spain (AEI)/European Regional Development Fund (ERDF) /10.13039/501100011033. We thank our four reviewers for their abundant and constructive comments.

Declaration of interest. The authors declare none.

References

- Aleksans J, Koehn D, Toussaint R and Daniel G (2020) Simulating hydraulic fracturing: failure in soft versus hard rocks. *Pure and Applied Geophysics* **177**, 2771–89.
- Anderson EM (1905) The dynamics of faulting. *Transactions of the Edinburgh Geological Society* **8**, 387–402.
- Anderson EM (1939) The dynamics of sheet intrusion. *Proceedings of the Royal Society of Edinburgh* **58**, 242–51.
- Anderson EM (1951) *The Dynamics of Faulting*. 2nd ed., Edinburgh: Oliver & Boyd.
- André A-S, Sausse J and Lespinaise M (2001) New approach for the quantification of paleostress magnitudes: application to the Soultz vein system (Rhine Graben, France). *Tectonophysics* **336**, 215–31.
- Atkinson BK (1984) Subcritical crack growth in geological materials. *Journal of Geophysical Research*, **89**, 4077–114.
- Bak P, Tang C and Wiesenfeld K (1988) Self-organized criticality. *Physical Review A* **38**, 364–74.
- Barnett W (2004) Subsidence breccias in kimberlite pipes: an application of fractal analysis. *Lithos* **76**, 299–316.
- Bear J (1988) *Dynamics of Fluids in Porous Media*. New York: Dover, 764 pp.
- Becker SP, Eichhubl P, Laubach SE, Reed RM, Lander RH and Bodnar RJ (2010) A 48 m.y. history of fracture opening, temperature, and fluid pressure: Cretaceous Travis Peak Formation, East Texas basin. *GSA Bulletin* **122**, 1081–93.
- Behrmann JH (1991) Conditions for hydrofracture and the fluid permeability of accretionary wedges. *Earth and Planetary Science Letters* **107**, 550–8.
- Bennion DB, Thomas FB and Bietz RF (1996) Low permeability gas reservoirs: problems, opportunities and solutions for drilling, completion, stimulation and production. In *SPE Gas Technology Symposium, Calgary, Alberta, Canada*, paper no. SPE-35577. Society of Petroleum Engineers.
- Biot MA (1941) General theory of three-dimensional consolidation. *Journal of Applied Physics* **12**, 155–64.
- Biot MA (1956) General solutions of the equations of elasticity and consolidation for a porous material. *Journal of Applied Mechanics* **23**, 91–6.
- Blenkinsop TG (1991) Cataclasis and processes of particle size reduction. *Pure and Applied Geophysics* **136**, 59–86.
- Bons PD (2001) The formation of large quartz veins by rapid ascent of fluids in mobile hydrofractures. *Tectonophysics* **336**, 1–17.
- Bons PD, Becker JK, Elburg MA and Urtson K (2009) Granite formation: stepwise accumulation of melt or connected networks? *Earth and Environmental Science Transactions of the Royal Society of Edinburgh* **100**, 105–15.
- Bons PD, Dougherty-Page J and Elburg MA (2001) Stepwise accumulation and ascent of magmas. *Journal of Metamorphic Geology* **19**, 627–33.
- Bons PD, Druguet E, Castaño LM and Elburg MA (2008) Finding what is not there anymore: recognizing missing fluid and magma volumes. *Geology* **36**, 851–4.

- Bons PD, Elburg MA and Gomez-Rivas E** (2012) A review of the formation of tectonic veins and their microstructures. *Journal of Structural Geology* **43**, 33–62.
- Bons PD, Fusswinkel T, Gomez-Rivas E, Markl G, Wagner T and Walter B** (2014) Fluid mixing from below in unconformity-related hydrothermal ore deposits. *Geology* **42**, 1035–8.
- Bons PD and Jessell MW** (1997) Experimental simulation of the formation of fibrous veins by localised dissolution-precipitation creep. *Mineralogical Magazine* **61**, 53–63.
- Bons PD and Montenari M** (2005) The formation of antitaxial calcite veins with well-developed fibres, Oppaminda Creek, South Australia. *Journal of Structural Geology* **27**, 231–48.
- Bons PD, Montenari M, Bakker RJ and Elburg MA** (2007) Potential evidence of Neoproterozoic deep life: SEM observations on calcite veins from Oppaminda Creek, Arkaroola, South Australia. *International Journal of Earth Sciences* **98**, 327–43.
- Bons PD and van Milligen BP** (2001) New experiment to model self-organized critical transport and accumulation of melt and hydrocarbons from their source rocks. *Geology* **29**, 919–22.
- Bourne SJ** (2003) Contrast of elastic properties between rock layers as a mechanism for the initiation and orientation of tensile failure under uniform remote compression. *Journal of Geophysical Research: Solid Earth* **108**, 2395. doi: [10.1029/2001JB001725](https://doi.org/10.1029/2001JB001725).
- Brederhoeft JD, Wolff RG, Keys WS and Shuter E** (1976) Hydraulic fracturing to determine the regional in situ stress field, Piceance Basin, Colorado. *Geological Society of America Bulletin* **87**, 250–8.
- Buckland W and De La Beche HT** (1835) I. – On the geology of the neighbourhood of Weymouth and the adjacent parts of the coast of Dorset. *Transactions of the Geological Society of London* **2–4**, 1–46.
- Cartwright JA** (1994) Episodic basin-wide fluid expulsion from geopressed shale sequences in the North Sea basin. *Geology* **22**, 447–50.
- Caswell TE and Milliken RE** (2017) Evidence for hydraulic fracturing at Gale crater, Mars: implications for burial depth of the Yellowknife Bay formation. *Earth and Planetary Science Letters* **468**, 72–84.
- Chauvet A** (2019) Structural control of ore deposits: the role of pre-existing structures on the formation of mineralised vein systems. *Minerals* **9**, 56.
- Clark JB** (1949) A hydraulic process for increasing the productivity of wells. *Journal of Petroleum Technology* **1**, 1–8.
- Cleary MP and Wong SK** (1985) Numerical simulation of unsteady fluid flow and propagation of a circular hydraulic fracture. *International Journal for Numerical and Analytical Methods in Geomechanics* **9**, 1–14.
- Clemens JD and Mawer CK** (1992) Granitic magma transport by fracture propagation. *Tectonophysics* **204**, 339–60.
- Cobbold PR and Rodrigues N** (2007) Seepage forces, important factors in the formation of horizontal hydraulic fractures and bedding-parallel fibrous veins (“beef” and “cone-in-cone”). *Geofluids* **7**, 313–22.
- Cobbold PR, Zanella A, Rodrigues N and Løseth H** (2013) Bedding-parallel fibrous veins (beef and cone-in-cone): worldwide occurrence and possible significance in terms of fluid overpressure, hydrocarbon generation and mineralization. *Marine and Petroleum Geology* **43**, 1–20.
- Connolly JAD** (1997) Devolatilization-generated fluid pressure and deformation-propagated fluid flow during prograde regional metamorphism. *Journal of Geophysical Research: Solid Earth* **102**, 18149–73.
- Cosgrove JW** (2001) Hydraulic fracturing during the formation and deformation of a basin: a factor in the dewatering of low-permeability sediments. *AAPG Bulletin* **85**, 7327–748.
- Cox SF** (1987) Antitaxial crack-seal vein microstructures and their relationship to displacement paths. *Journal of Structural Geology* **9**, 779–87.
- Cox SF** (1995) Faulting processes at high fluid pressures: an example of fault valve behavior from the Wattle Gully Fault, Victoria, Australia. *Journal of Geophysical Research: Solid Earth* **100**, 12841–59.
- Cox SF** (2005) Coupling between deformation, fluid pressures, and fluid flow in ore-producing hydrothermal systems at depth in the crust. In *100th Anniversary Volume*, pp. 39–75. Littleton, Colorado: Society of Economic Geologists.
- Cox SF** (2010) The application of failure mode diagrams for exploring the roles of fluid pressure and stress states in controlling styles of fracture-controlled permeability enhancement in faults and shear zones. *Geofluids* **10**, 217–33.
- Cox SF, Etheridge MA and Wall VJ** (1986) The role of fluids in syntectonic mass transport, and the localization of metamorphic vein-type ore deposits. *Ore Geology Reviews* **2**, 65–86.
- Dahm T** (2000) On the shape and velocity of fluid-filled fractures in the Earth. *Geophysical Journal International* **142**, 181–92.
- Dahm T, Hainzl S and Fischer T** (2010) Bidirectional and unidirectional fracture growth during hydrofracturing: role of driving stress gradients. *Journal of Geophysical Research* **115**, B12322.
- de Boer R and Ehlers W** (1988) A historical review of the formulation of porous media theories. *Acta Mechanica* **74**, 1–8.
- de Boer R and Ehlers W** (1990) The development of the concept of effective stress. *Acta Mechanica* **83**, 77–92.
- de Riese T, Bons PD, Gomez-Rivas E and Sachau T** (2020) Interaction between crustal-scale Darcy and hydrofracture fluid transport: a numerical study. *Geofluids* **2020**, 1–14.
- Delaney PT, Pollard DD, Zioney JI and McKee EH** (1986) Field relations between dikes and joints: emplacement processes and paleostress analysis. *Journal of Geophysical Research* **91**, 4920e4983. doi: [10.1029/JB091iB05p04920](https://doi.org/10.1029/JB091iB05p04920).
- Durney DW and Ramsay JG** (1973) Incremental strains measured by syntectonic crystal growths. In *Gravity and Tectonics* (eds KA De Jong and R Scholten), pp. 67–96. New York: Wiley.
- Eichhubl P** (2000) Rates of fluid flow in fault systems; evidence for episodic rapid fluid flow in the Miocene Monterey Formation, coastal California. *American Journal of Science* **300**, 571–600.
- Engelder T** (1999) Transitional–tensile fracture propagation: a status report. *Journal of Structural Geology* **21**, 1049–55.
- Engelder T and Lacazette A** (1990) Natural hydraulic fracturing. In *Rock Joints* (eds N Barton and O Stephansson), pp. 35–44. Rotterdam: A.A. Balkema.
- Etheridge MA** (1983) Differential stress magnitudes during regional deformation and metamorphism: upper bound imposed by tensile fracturing. *Geology* **11**, 231–4.
- Fall A, Eichhubl P, Bodnar RJ, Laubach SE and Davis JS** (2015) Natural hydraulic fracturing of tight-gas sandstone reservoirs, Piceance Basin, Colorado. *GSA Bulletin* **127**, 61–75.
- Fillunger P** (1936) *Erdbaumechanik?* Vienna: Selbstverlag des Verfassers, 31 pp.
- Fisher DM and Brantley SL** (1992) Models of quartz overgrowth and vein formation: deformation and episodic fluid flow in an ancient subduction zone. *Journal of Geophysical Research* **97**, 20043.
- Flekkøy EG** (2002) Modeling hydrofracture. *Journal of Geophysical Research* **107**, 2151.
- Fletcher RC and Merino E** (2001) Mineral growth in rocks: kinetic-rheological models of replacement, vein formation, and syntectonic crystallization. *Geochimica et Cosmochimica Acta* **65**, 3733–48.
- Gale JFW, Lander RH, Reed RM and Laubach SE** (2010) Modeling fracture porosity evolution in dolostone. *Journal of Structural Geology* **32**, 1201–11.
- Gehne S and Benson PM** (2019) Permeability enhancement through hydraulic fracturing: laboratory measurements combining a 3D printed jacket and pore fluid over-pressure. *Scientific Reports* **9**, 12573.
- Ghani I, Koehn D, Toussaint R and Passchier CW** (2013) Dynamic development of hydrofracture. *Pure and Applied Geophysics* **170**, 1685–703.
- Ghani I, Koehn D, Toussaint R and Passchier CW** (2015) Dynamics of hydrofracturing and permeability evolution in layered reservoirs. *Frontiers in Physics* **3**, 67.
- Gibiansky L and Torquato S** (1998) Rigorous connection between physical properties of porous rocks. *Journal of Geophysical Research* **103**, 23911–23.
- Goldfarb RJ, Snee LW and Pickthorn WJ** (1993) Orogenesis, high-T thermal events, and gold vein formation within metamorphic rocks of the Alaskan Cordillera. *Mineralogical Magazine* **57**, 375–94.
- Gomez-Rivas E, Bons PD, Koehn D, Urai JL, Arndt M, Virgo S, Laurich B, Zeeb C, Stark L and Blum P** (2014) The Jabal Akhdar dome in the Oman Mountains: evolution of a dynamic fracture system. *American Journal of Science* **314**, 1104–39.
- Gomez-Rivas E and Griera A** (2012) Shear fractures in anisotropic ductile materials: an experimental approach. *Journal of Structural Geology* **34**, 61–76.

- González-Esvertit E, Canals A, Bons PD, Casas JM and Gomez-Rivas E** (2022) Compiling regional structures in geological databases: the Giant Quartz Veins of the Pyrenees as a case study. *Journal of Structural Geology* **163**, 104705. doi: [10.1016/j.jsg.2022.104705](https://doi.org/10.1016/j.jsg.2022.104705).
- Gordayev Yu N and Zazovsky AF** (1992) Self-similar solution for deep-penetrating hydraulic fracture propagation. *Transport in Porous Media* **7**, 283–304.
- Goren L, Aharonov E, Sparks D and Toussaint R** (2010) Pore pressure evolution in deforming granular material: a general formulation and the infinitely stiff approximation. *Journal of Geophysical Research* **115**, B09216.
- Goren L, Aharonov E, Sparks D and Toussaint R** (2011) The mechanical coupling of fluid-filled granular material under shear. *Pure and Applied Geophysics* **168**, 2289–323.
- Griffith A** (1924) The theory of rupture. In *Proceedings of the 1st International Congress of Applied Mechanics, Delft* (eds CB Biereno and JM Burgers), Delft: Tech. Boekhandel en Drukkerij. J. Waltman Jr. pp. 54–63.
- Griffith AA** (1920) The phenomena of rupture and flow in solids. *Philosophical Transactions: Royal Society, London, Series A* **221**, 163–98.
- Groves DI, Santosh M, Goldfarb RJ and Zhang L** (2018) Structural geometry of orogenic gold deposits: implications for exploration of world-class and giant deposits. *Geoscience Frontiers* **9**, 1163–77.
- Gudmundsson A** (2011) *Rock Fractures in Geological Processes*. Cambridge: Cambridge University Press, 592 pp.
- Guerrero V and Mazzoli S** (2021) Theory of effective stress in soil and rock and implications for fracturing processes: a review. *Geosciences* **11**, 119.
- He Q, Suorinen FT and Oh J** (2016) Review of hydraulic fracturing for pre-conditioning in cave mining. *Rock Mechanics and Rock Engineering* **49**, 4893–910.
- Hilgers C, Koehn D, Bons PD and Urai J** (2001) Development of crystal morphology during uniaxial growth in a progressively widening vein: II. Numerical simulations of the evolution of antitaxial fibrous veins. *Journal of Structural Geology* **23**, 873–85.
- Hillis RR** (2003) Pore pressure/stress coupling and its implications for rock failure. In *Subsurface Sediment Mobilization* (eds JJ Maltman & CK Morley), pp. 359–68. *Geological Society of London, Special Publication* no. **216**.
- Hooker JN and Fisher, DM** 2021. How cementation and fluid flow influence slip behaviour at the subduction interface. *Geology* **49**, 1074–8.
- Hooker JN, Larson TE, Eakin A, Laubach SE, Eichhubl P, Fall A and Marrett R** (2015) Fracturing and fluid flow in a sub-décollement sandstone; or, leak in the basement. *Journal of the Geological Society* **172**, 428–42.
- Hooker JN, Ruhl M, Dickson AJ, Hansen LN, Idiz E, Hesselbo SP and Cartwright J** (2020) Shale anisotropy and natural hydraulic fracture propagation: an example from the Jurassic (Toarcian) Posidonienschiefer, Germany. *Journal of Geophysical Research: Solid Earth*, **125**, e2019JB018442. doi: [10.1029/2019JB018442](https://doi.org/10.1029/2019JB018442).
- Hubbert MK** (1951) Mechanical basis for certain familiar geologic structures. *Geological Society of America Bulletin* **62**, 355–72.
- Hubbert MK and Rubey WW** (1959) Role of fluid pressure in mechanics of overthrust faulting: I. Mechanics of fluid-filled porous solids and its application to overthrust faulting. *Geological Society of America Bulletin* **70**, 115–66.
- Hunt JM** (1990) Generation and migration of petroleum from abnormally pressured fluid compartments. *AAPG Bulletin* **74**, 1–12.
- Ingebritsen SE and Manning CE** (1999) Geological implications of a permeability-depth curve for the continental crust. *Geology* **27**, 1107–10.
- Inglis CE** (1913) Stresses in plates due to the presence of cracks and sharp corners. *Transactions of the Institute of Naval Architects* **55**, 219–41.
- Jaeger JC, Cook NGW and Zimmerman R** (2007) *Fundamentals of Rock Mechanics*. Chichester: Wiley.
- Jaques L and Pascal C** (2017) Full paleostress tensor reconstruction using quartz veins of Panasqueira Mine, central Portugal; part I: paleopressure determination. *Journal of Structural Geology* **102**, 58–74.
- Jébrak M** (1997) Hydrothermal breccias in vein-type ore deposits: a review of mechanisms, morphology and size distribution. *Ore Geology Reviews* **12**, 111–34.
- Johnsen Ø, Chevalier C, Lindner A, Toussaint R, Clément E, Måløy KJ, Flekkøy EG and Schmittbuhl J** (2008b) Decompaction and fluidization of a saturated and confined granular medium by injection of a viscous liquid or gas. *Physical Review E* **78**, 051302.
- Johnsen Ø, Toussaint R, Måløy KJ and Flekkøy EG** (2006) Pattern formation during air injection into granular materials confined in a circular Hele-Shaw cell. *Physical Review E* **74**, 011301.
- Johnsen Ø, Toussaint R, Måløy KJ, Flekkøy EG and Schmittbuhl J** (2008a) Coupled air/granular flow in a linear Hele-Shaw cell. *Physical Review E* **77**, 011301.
- Jolly RJH and Sanderson DJ** (1997) A Mohr circle construction for the opening of a pre-existing fracture. *Journal of Structural Geology* **19**, 887–92.
- Katsaga T, Riahi A, DeGagne DO, Valley B and Damjanac B** (2015) Hydraulic fracturing operations in mining: conceptual approach and DFN modeling example. *Mining Technology* **124**, 255–66.
- Keulen N, Heilbronner R, Stünitz H, Boullier A-M and Ito H** (2007) Grain size distributions of fault rocks: a comparison between experimentally and naturally deformed granitoids. *Journal of Structural Geology* **29**, 1282–300.
- Kling T, Schwarz J-O, Wendler F, Enzmann F and Blum P** (2017) Fracture flow due to hydrothermally induced quartz growth. *Advances in Water Resources*, **107**, 93–107.
- Koehn D, Arnold J and Passchier CW** (2005) Fracture and vein patterns as indicators of deformation history: a numerical study. In *Deformation Mechanisms, Rheology and Tectonics from Minerals to the Lithosphere* (eds D Gapais, J-P Brun and PR Cobbold), pp. 11–24. Geological Society of London, Special Publication no. 243.
- Koehn D, Piaolo S, Sachau T and Toussaint R** (2020) Fracturing and porosity channeling in fluid overpressure zones in the shallow earth's crust. *Geofluids* **2020**, 1–17.
- Kronyak RE, Kah LC, Edgett KS, Van Bommel SJ, Thompson LM, Wiens RC, Sun VZ and Nachon M** (2019) Mineral-filled fractures as indicators of multigenerational fluid flow in the Pahrump Hills member of the Murray formation, Gale crater, Mars. *Earth and Space Science* **6**, 238–65.
- Krueger RF** (1973) Advances in well completion and stimulation during JPT's first quarter century. *Journal of Petroleum Technology* **25**, 1447–62.
- Lander RH and Laubach SE** (2015) Insight into rates of fracture growth and sealing for a model for quartz cementation in fractures sandstones. *GSA Bulletin* **127**, 516–38.
- Laubach SE, Lander RH, Criscenti LJ, Anovitz LM, Urai JL, Pollyea RM, Hooker JN, Narr W, Evans MA, Kerisit SN, Olson JE, Dewers T, Fisher D, Bodnar R, Evans B, Dove P, Bonnell LM, Marder MP and Pyrak-Nolte L** (2019) The role of chemistry in fracture pattern development and opportunities to advance interpretations of geological materials. *Reviews of Geophysics* **57**, 1065–111.
- Laubach SE, Reed RM, Olson JE, Lander RH and Bonnell LM** (2004) Coevolution of crack-seal texture and fracture porosity in sedimentary rocks: cathodoluminescence observations of regional fractures. *Journal of Structural Geology* **26**, 967–82.
- Laznicka P** (1989) Breccias and ores. Part 1: history, organization and petrography of breccias. *Ore Geology Reviews* **4**, 315–44.
- Lister JR and Kerr RC** (1991) Fluid-mechanical models of crack propagation and their application to magma transport in dykes. *Journal of Geophysical Research* **96**, 10049–77.
- Lister JR and Kerr RC** (1990) Fluid-mechanical models of dyke propagation and magma transport. In *Mafic Dykes and Emplacement Mechanisms* (eds AJ Parker, PC Rickwood and DH Tucker), pp. 69–80. Rotterdam: Balkema.
- Liu X, Xing H and Zhang D** (2017) Influences of hydraulic fracturing on fluid flow and mineralization at the vein-type tungsten deposits in Southern China. *Geofluids* **2017**, 1–11.
- Lorilleux G, Jébrak M, Cuney M and Baudemont D** (2002) Polyphase hydrothermal breccias associated with unconformity-related uranium mineralization (Canada): from fractal analysis to structural significance. *Journal of Structural Geology* **24**, 323–38.
- Luan G, Dong C, Azmy K, Lin C, Ma C, Ren L and Zhu Z** (2019) Origin of bedding-parallel fibrous calcite veins in lacustrine black shale: a case study from Dongying Depression, Bohai Bay Basin. *Marine and Petroleum Geology* **102**, 873–85.
- Maaløe S** (1987) The generation and shape of feeder dykes from mantle sources. *Contributions to Mineralogy and Petrology* **96**, 47–55.
- MacDonald IR, Buthman DB, Sager WW, Peccini MB and Guinasso NL** (2000) Pulsed oil discharge from a mud volcano. *Geology* **28**, 907–10.

- Manning CE and Ingebritsen SE** (1999) Permeability of the continental crust: implications of geothermal data and metamorphic systems. *Reviews of Geophysics* **37**, 127–50.
- Marchildon N and Brown M** (2003) Spatial distribution of meltbearing structures in anatectic rocks from Southern Brittany, France: implications for melt transfer at grain- to orogen-scale. *Tectonophysics* **364**, 215–35.
- Matthäi SK, Heinrich CA and Driesner T** (2004) Is the Mount Isa copper deposit the product of forced brine convection in the footwall of a major reverse fault? *Geology* **32**, 357–60.
- Means WD and Li T** (2001) A laboratory simulation of fibrous veins: some first observations. *Journal of Structural Geology* **23**, 857–63.
- Meng Q, Hooker J and Cartwright J** (2019) Role of pressure solution in the formation of bedding-parallel calcite veins in an immature shale (Cretaceous, southern UK). *Geological Magazine* **156**, 918–34.
- Meyer BR** (1986) Design formulae for 2-D and 3-D vertical hydraulic fractures: model comparison and parametric studies. In *SPE Unconventional Gas Technology Symposium*, SPE 15240. Louisville, Kentucky. Society of Petroleum Engineers.
- Miller SA and Nur A** (2000) Permeability as a toggle switch in fluid-controlled crustal processes. *Earth and Planetary Science Letters* **183**, 133–46.
- Mohr O** (1882) Über die Darstellung des Spannungszustandes eines Korpelementes. *Zivil Ingenieure* **28**, 113.
- Montgomery CT and Smith MB** (2010) Hydraulic fracturing: history of an enduring technology. *Journal of Petroleum Technology* **62**, 26–40.
- Mort K and Woodcock NH** (2008) Quantifying fault breccia geometry: Dent Fault, NW England. *Journal of Structural Geology* **30**, 701–9.
- Moska R, Labus K and Kasza P** (2021) Hydraulic fracturing in enhanced geothermal systems – field, tectonic and rock mechanics conditions: a review. *Energies* **14**, 5725.
- Mügge O** (1928) Über die Entstehung faseriger Minerale und ihrer Aggregationsformen. *Neues Jahrbuch für Mineralogie, Geologie und Paläontologie* **58A**, 303–48.
- Nakashima Y** (1993) Buoyancy-driven propagation of an isolated fluid-filled crack in rock: implication for fluid transport in metamorphism. *Contributions to Mineralogy and Petrology* **114**, 289–95.
- Niebling MJ, Flekkøy EG, Måløy KJ and Toussaint R** (2010a) Mixing of a granular layer falling through a fluid. *Physical Review E* **82**, 011301.
- Niebling MJ, Flekkøy EG, Måløy KJ and Toussaint R** (2010b) Sedimentation instabilities: impact of the fluid compressibility and viscosity. *Physical Review E* **82**, 051302.
- Nor A and Walder J** (1992) Hydraulic pulses in the Earth's crust. In *International Geophysics* (eds B Evans and T-F Wong), pp. 461–73. Amsterdam: Elsevier.
- Nunn JA** (1996) Buoyancy-driven propagation of isolated fluid-filled fractures: implications for fluid transport in Gulf of Mexico geopressed sediments. *Journal of Geophysical Research: Solid Earth* **101**, 2963–70.
- Nur A and Byerlee JD** (1971) An exact effective stress law for elastic deformation of rock with fluids. *Journal of Geophysical Research* **76**, 6414–19.
- Okamoto A and Sekine K** (2011) Textures of syntaxial quartz veins synthesized by hydrothermal experiments. *Journal of Structural Geology* **33**, 1764–75.
- Okamoto A and Tsuchiya N** (2009) Velocity of vertical fluid ascent within vein-forming fractures. *Geology* **37**, 563–6.
- Oliver J** (1986) Fluids expelled tectonically from orogenic belts: their role in hydrocarbon migration and other geologic phenomena. *Geology* **14**, 99–102.
- Oliver NHS and Bons PD** (2001) Mechanisms of fluid flow and fluid-rock interaction in fossil metamorphic hydrothermal systems inferred from vein-wallrock patterns, geometry and microstructure. *Geofluids* **1**, 137–62.
- Oliver NHS, McLellan JG, Hobbs BE, Cleverley JS, Ord A and Feltrin L** (2006a) 100th anniversary special paper: numerical models of extensional deformation, heat transfer, and fluid flow across basement-cover interfaces during basin-related mineralization. *Economic Geology* **101**, 1–31.
- Oliver NHS, Rubenach MJ, Fu B, Baker T, Blenkinsop TG, Cleverley JS, Marshall LJ and Ridd PJ** (2006b) Granite-related overpressure and volatile release in the mid crust: fluidized breccias from the Cloncurry District, Australia. *Geofluids* **6**, 346–58.
- Olson JE, Laubach SE and Lander RH** (2009) Natural fracture characterization in tight gas sandstones: integrating mechanics and diagenesis. *AAPG Bulletin* **93**, 1535–49.
- Osborne MJ and Swarbrick RE** (1997) Mechanisms for generating overpressure in sedimentary basins: a reevaluation. *AAPG Bulletin* **81**, 1023–41.
- Pascal C** (2021) *Paleostress Inversion Techniques: Methods and Applications for Tectonics*. Amsterdam: Elsevier, 274 pp.
- Passchier CW and Trouw RAJ** (2005) *Microtectonics* 2nd, rev.enl. edn. Berlin and New York: Springer, 366 pp.
- Pati JK, Patel SC, Pruseth KL, Malviya VP, Arima M, Raju S, Pati P and Prakash K** (2007) Geology and geochemistry of giant quartz veins from the Bundelkhand Craton, central India and their implications. *Journal of Earth System Science* **116**, 497–510.
- Person M, Mulch A, Teyssier C and Gao Y** (2007) Isotope transport and exchange within metamorphic core complexes. *American Journal of Science* **307**, 555–89.
- Petford N, Kerr RC and Lister JR** (1993) Dike transport of granitoid magmas. *Geology* **21**, 845–8.
- Pettke T and Diamond LW** (1996) Oligocene gold quartz veins at Brusson, NW Alps: Sr isotopes trace the source of ore-bearing fluid to over a 10-km depth. *Economic Geology* **92**, 389–406.
- Phillip S** (2012) Fluid overpressure estimates from the aspect ratios of mineral veins. *Tectonophysics* **581**, 35–47.
- Phillips WJ** (1972) Hydraulic fracturing and mineralization. *Journal of the Geological Society* **128**, 337–59.
- Pirajno F** (2009) Hydrothermal processes and wall rock alteration. In *Hydrothermal Processes and Mineral Systems* (ed. F Pirajno), pp. 73–164. Dordrecht: Springer.
- Pollard DD** (1976) On the form and stability of open hydraulic fractures in the Earth's crust. *Geophysical Research Letters* **3**, 513–16.
- Pollard DD and Aydin A** (1988) Progress in understanding jointing over the past century. *Geological Society of America Bulletin* **100**, 1181–204.
- Pollard PD and Fletcher RC** (2005) *Fundamentals of Structural Geology*. Cambridge: Cambridge University Press, 514 pp.
- Preisig G, Eberhardt E, Gischig V, Roche V, van der Baan M, Valley B, Kaiser PK, Duff D and Lowther R** (2016) Development of connected permeability in massive crystalline rocks through hydraulic fracture propagation and shearing accompanying fluid injection. In *Crustal Permeability* (eds T Gleeson and SE Ingebritse), pp. 335–52. Chichester: John Wiley & Sons, Ltd.
- Ramsay JG** (1980) The crack–seal mechanism of rock deformation. *Nature* **284**, 135–9.
- Ramsey JM and Chester FM** (2004) Hybrid fracture and the transition from extension fracture to shear fracture. *Nature* **428**, 63–6.
- Regenauer-Lieb K** (1999) Dilatant plasticity applied to Alpine collision: ductile void growth in the intraplate area beneath the Eifel volcanic field. *Journal of Geodynamics* **27**, 1–21.
- Renard F, Andréani M, Boullier A-M and Labaume P** (2005) Crack-seal patterns: records of uncorrelated stress release variations in crustal rocks. In *Deformation Mechanisms, Rheology and Tectonics from Minerals to the Lithosphere* (eds D Gapais, J-P Brun and PR Cobbold), pp. 67–79. *Geological Society of London, Special Publication no. 243*.
- Rice CM, Mark DF, Selby D, Neilson JE and Davidheiser-Kroll B** (2016) Age and geologic setting of quartz vein-hosted gold mineralization at Curraghinalt, Northern Ireland: implications for genesis and classification. *Economic Geology* **111**, 127–50.
- Richard HA and Sander M** (2016) *Fatigue Crack Growth*. Cham: Springer Vieweg, 292 pp.
- Rivalta E, Böttlinger M and Dahm T** (2005) Buoyancy-driven fracture ascent: experiments in layered gelatine. *Journal of Volcanology and Geothermal Research* **144**, 273–85.
- Rivalta E, Taisne B, Bungler AP and Katz RF** (2015) A review of mechanical models of dike propagation: schools of thought, results and future directions. *Tectonophysics* **638**, 1–42.
- Rogatz H** (1961) Shallow oil & gas fields of the Texas Panhandle and Hugoton. In *Oil and Gas Fields of the Texas and Oklahoma Panhandles* (ed. RC Wagner), pp. 8–37. Amarillo, Texas: Panhandle (Texas) Geological Society.
- Rojstaczer SA, Ingebritsen SE and Hayba DO** (2008) Permeability of continental crust influenced by internal and external forcing. *Geofluids* **8**, 128–39.
- Roos DP and Cartwright DJ** (1976) *Compendium of Stress Intensity Factors*. London: Her Majesty's Stationery Office, 330 pp.

- Rubin AM** (1995) Propagation of magma-filled cracks. *Annual Review of Earth and Planetary Sciences* **23**, 287–336.
- Schaarschmidt A, Haase KM, de Wall H, Bestmann M, Krumm S and Regelous M** (2019) Upper crustal fluids in a large fault system: microstructural, trace element and oxygen isotope study on multi-phase vein quartz at the Bavarian Pfahl, SE Germany. *International Journal of Earth Sciences* **108**, 521–43.
- Secor DT** (1965) Role of fluid pressure in jointing. *American Journal of Science* **263**, 633–46.
- Secor DT and Pollard DD** (1975) On the stability of open hydraulic fractures in the Earth's crust. *Geophysical Research Letters* **2**, 510–13.
- Shapiro SA and Dinske C** (2009) Fluid-induced seismicity: pressure diffusion and hydraulic fracturing. *Geophysical Prospecting* **57**, 301–10.
- Sharp ZD, Masson H and Lucchini R** (2005) Stable isotope geochemistry and formation mechanisms of quartz veins; extreme paleoaltitudes of the Central Alps in the Neogene. *American Journal of Science* **305**, 187–219.
- Sibson RH** (1986) Brecciation processes in fault zones: inferences from earthquake rupturing. *Pure and Applied Geophysics* **124**, 159–75.
- Sibson RH** (2000a) Fluid involvement in normal faulting. *Journal of Geodynamics* **29**, 469–99.
- Sibson RH** (2000b) Tectonic controls on maximum sustainable overpressure: fluid redistribution from stress transitions. *Journal of Geochemical Exploration* **69–70**, 471–5.
- Sibson RH** (2003) Brittle-failure controls on maximum sustainable overpressure in different tectonic regimes. *AAPG Bulletin* **87**, 901–8.
- Sibson RH, Moore JMcM and Rankin AH** (1975) Seismic pumping: a hydrothermal fluid transport mechanism. *Journal of the Geological Society* **131**, 653–9.
- Sibson RH, Robert F and Poulsen KH** (1988) High-angle reverse faults, fluid-pressure cycling, and mesothermal gold-quartz deposits. *Geology* **16**, 551–5.
- Sih GC** (1973) *Stress-Intensity Factors for Researchers and Engineers*. Bethlehem, PA: Institute of Fracture and Solid Mechanics, Lehigh University.
- Skempton AW** (1960) Significance of Terzaghi's concept of effective stress (Terzaghi's discovery of effective stress). In *From Theory to Practice in Soil Mechanics* (eds L Bjerrum, A Casagrande, RB Peek and AW Skempton), pp. 42–53. New York and London: John Wiley & Sons.
- Sleep NH** (1988) Tapping of melt by veins and dikes. *Journal of Geophysical Research* **93**, 10255–72.
- Soloyev TM and Kobeleva VA** (1960) Ways to intensify oil production. *Petroleum Geology: A Digest of Russian Literature on Petroleum Geology* **4**, 661–5.
- Sornette D** (2009) Dragon-kings, black swans and the prediction of crises. *SSRN Electronic Journal* **2**, 1–18.
- Späth M, Spruženiec L, Urai JL, Selzer M, Arndt M and Nestler B** (2021) Kinematics of crystal growth in single-seal syntaxial veins in limestone: a phase-field study. *Journal of Geophysical Research: Solid Earth* **126**, e2021JB022106.
- Späth M, Urai JL and Nestler B** (2022) Incomplete crack sealing causes localization of fracturing in hydrothermal quartz veins. *Geophysical Research Letters* **49**, e2022GL098643.
- Spence DA and Turcotte DL** (1985) Magma-driven propagation of cracks. *Journal of Geophysical Research: Solid Earth* **90**, 575–80.
- Stanchits S, Mayr S, Shapiro S and Dresen G** (2011) Fracturing of porous rock induced by fluid injection. *Tectonophysics* **503**, 129–45.
- Staudé S, Bons PD and Markl G** (2009) Hydrothermal vein formation by extension-driven dewatering of the middle crust: an example from SW Germany. *Earth and Planetary Science Letters* **286**, 387–95.
- Stork AL, Verdon JP and Kendall J-M** (2015) The microseismic response at the In Salah Carbon Capture and Storage (CCS) site. *International Journal of Greenhouse Gas Control* **32**, 159–71.
- Su A, Bons PD, Chen H, Feng Y, Zhao J and Song J** (2021) Age, material source, and formation mechanism of bedding-parallel calcite beef veins: case from the mature Eocene lacustrine shales in the Biyang Sag, Nanxiang Basin, China. *GSA Bulletin* **134**, 1811–33.
- Sun Z, Wang J, Wang Y, Zhang Y and Zhao L** (2021) Multistage hydrothermal quartz veins record the ore-forming fluid evolution in the Meiling Cu–Zn (Au) deposit, NW China. *Ore Geology Reviews* **131**, 104002.
- Taber S** (1918) The origin of veinlets in the Silurian and Devonian strata of Central New York. *The Journal of Geology* **26**, 56–73.
- Takada A** (1990) Experimental study on propagation of liquid-filled crack in gelatin: shape and velocity in hydrostatic stress condition. *Journal of Geophysical Research* **95**, 8471.
- Terzaghi K** (1923) Die Berechnung der Durchlässigkeit des Tones aus dem Verlauf der hydromechanischen Spannungserscheinungen. *Sitzungsberichte der Kaiserlichen Akademie der Wissenschaften (Wien), Mathematisch-Naturwissenschaftliche Klasse* **132**, 125–38.
- Terzaghi K** (1943) *Theoretical Soil Mechanics*. New York and London: John Wiley and Sons, 510 pp.
- Townend J and Zoback MD** (2000) How faulting keeps the crust strong. *Geology* **28**, 399–402.
- Turcotte DL** (1986) Fractals and fragmentation. *Journal of Geophysical Research* **91**, 1921–6.
- Turcotte DL** (1999) Self-organized criticality. *Reports on Progress in Physics* **62**, 1377–429.
- Tzschichholz F, Herrmann HJ, Roman HE and Pfuff M** (1994) Beam model for hydraulic fracturing. *Physical Review B* **49**, 7056–9.
- Urai JL, Williams PF and van Roermund HLM** (1991) Kinematics of crystal growth in syntectonic fibrous veins. *Journal of Structural Geology* **13**, 823–36.
- US Nuclear Regulatory Commission** (2009) Generic environmental impact statement for in-situ leach uranium milling facilities. Office of Federal and State Materials and Environmental Management Programs. Land Quality Division, Wyoming Department of Environmental Quality. Available at: www.nrc.gov/reading-rm.html (Last Access: Nov 2022).
- Vass A, Koehn D, Toussaint R, Ghani I and Piazzolo S** (2014) The importance of fracture-healing on the deformation of fluid-filled layered systems. *Journal of Structural Geology* **67**, 94–106.
- Vielreicher NM, Groves DI and McNaughton NJ** (2016) The giant Kalgoorlie Gold Field revisited. *Geoscience Frontiers* **7**, 359–74.
- Vinningland JL, Johnsen Ø, Flekkøy EG, Toussaint R and Måløy KJ** (2007a) Experiments and simulations of a gravitational granular flow instability. *Physical Review E* **76**, 051306.
- Vinningland JL, Johnsen Ø, Flekkøy EG, Toussaint R and Måløy KJ** (2007b) Granular Rayleigh-Taylor instability: experiments and simulations. *Physical Review Letters* **99**, 048001.
- Vinningland JL, Johnsen Ø, Flekkøy EG, Toussaint R and Måløy KJ** (2010) Size invariance of the granular Rayleigh-Taylor instability. *Physical Review E* **81**, 041308.
- Vinningland JL, Toussaint R, Niebling M, Flekkøy EG and Måløy KJ** (2012) Family-Vicsek scaling of detachment fronts in granular Rayleigh-Taylor instabilities during sedimentating granular/fluid flows. *The European Physical Journal Special Topics* **204**, 27–40.
- Virgo S, Abe S and Urai JL** (2014) The evolution of crack seal vein and fracture networks in an evolving stress field: insights from Discrete Element Models of fracture sealing: DEM crack-seal evolution. *Journal of Geophysical Research: Solid Earth* **119**, 8708–27.
- Walder J and Nur A** (1984) Porosity reduction and crustal pore pressure development. *Journal of Geophysical Research: Solid Earth* **89**, 11539–48.
- Wang M, Chen Y, Song G, Steele-MacInnis M, Liu Q, Wang X, Zhang X, Zhao Z, Liu W, Zhang H and Zhou Z** (2018) Formation of bedding-parallel, fibrous calcite veins in laminated source rocks of the Eocene Dongying Depression: a growth model based on petrographic observations. *International Journal of Coal Geology* **200**, 18–35.
- Wang Q, Chen X, Jha AN and Rogers H** (2014) Natural gas from shale formation: the evolution, evidences and challenges of shale gas revolution in United States. *Renewable and Sustainable Energy Reviews* **30**, 1–28.
- Wangen M** (2022) A model of fluid expulsion from compacting tight sedimentary rocks based on the Toggle-Switch algorithm. *Applied Computing and Geosciences* **13**, 100079.
- Weertman J** (1971) Theory of water-filled crevasses in glaciers applied to vertical magma transport beneath oceanic ridges. *Journal of Geophysical Research* **76**, 1171–83.
- Weinberg RF and Regenauer-Lieb K** (2010) Ductile fractures and magma migration from source. *Geology* **38**, 363–6.
- Weis P** (2015) The dynamic interplay between saline fluid flow and rock permeability in magmatic-hydrothermal systems. *Geofluids* **15**, 350–71.

- Weisheit A, Bons PD, Danišik M and Elburg MA** (2013b) Crustal-scale folding: palaeozoic deformation of the Mt Painter Inlier, South Australia. In *Deformation Structure and Processes within the Continental Crust* (eds S Llana-Funez, A Marcos and F Bastida), pp. 53–77. *Geological Society of London, Special Publication* no. 394.
- Weisheit A, Bons PD and Elburg MA** (2013a) Long-lived crustal-scale fluid flow: the hydrothermal mega-breccia of Hidden Valley, Mt. Painter Inlier, South Australia. *International Journal of Earth Sciences* **102**, 1219–36.
- Westergaard HM** (1939) Bearing pressures and cracks. *Journal of Applied Mechanics* **6**, A49–53.
- Wiltschko DV and Morse JW** (2001) Crystallization pressure versus “crack seal” as the mechanism for banded veins. *Geology* **29**, 79–82.
- Xiong Y, Zuo R, Clarke KC, Miller SA and Wang J** (2020) Modeling singular mineralization processes due to fluid pressure fluctuations. *Chemical Geology* **535**, 119458.
- Yamaji A, Sato K and Tonai S** (2010) Stochastic modeling for the stress inversion of vein orientations: paleostress analysis of Pliocene epithermal veins in southwestern Kyushu, Japan. *Journal of Structural Geology* **32**, 1137–46.
- Yardley BWD** (1986) Fluid migration and veining in the Connemara Schists, Ireland. In *Fluid—Rock Interactions during Metamorphism* (eds JV Walther and BJ Wood), pp. 109–31. New York: Springer.
- Zanella A, Cobbold PR and Boassen T** (2015a) Natural hydraulic fractures in the Wessex Basin, SW England: widespread distribution, composition and history. *Marine and Petroleum Geology* **68**, 438–48.
- Zanella A, Cobbold PR, Ruffet G and Leanza HA** (2015b) Geological evidence for fluid overpressure, hydraulic fracturing and strong heating during maturation and migration of hydrocarbons in Mesozoic rocks of the northern Neuquén Basin, Mendoza Province, Argentina. *Journal of South American Earth Sciences* **62**, 229–42.
- Zhang B, Yin C, Gu Z, Zhang J, Yan S and Wang Y** (2015) New indicators from bedding-parallel beef veins for the fault valve mechanism. *Science China Earth Sciences* **58**, 1320–36.
- Zhao C, Hobbs BE and Ord A** (2008) *Convective and Advective Heat Transfer in Geological Systems*. Berlin and London: Springer, 229 pp.
- Zhu Q-Z** (2017) A new rock strength criterion from microcracking mechanisms which provides theoretical evidence of hybrid failure. *Rock Mechanics and Rock Engineering* **50**, 341–52.